In Conventional Weapons Underwater Explosions, pages 43-83. Office of Naval Research, Dec 1988.
Workshop Report ONR Contract No. N00014-88-J-1150.

Interface Effects in Underwater Explosions

J. E. Shepherd

August 31, 1988

Rensselaer Polytechnic Institute
Department of Mechanical Engineering,
Aeronautical Engineering and Mechanics
Troy, NY

ONR/GIT Workshop on Underwater Explosions
Atlanta, Georgia
August 2-3, 1988

Interface Effects in Underwater Explosions

J. E. Shepherd

Rensselaer Polytechnic Institute
Department of Mechanical Engineering,
Aeronautical Engineering and Mechanics
Troy, NY

Abstract

The interface between explosive products and the surrounding water plays an important role in underwater explosion phenomena. The effects of the energy and mass transfer processes occurring at the interface significantly influence shock wave production, bubble oscillation, migration and interaction with adjacent surfaces. Density and impedance differences across the interface are factors in determining the initial shock wave strength and the subsequent decay. Superheated water is created due to shock heating and bubble overexpansion during oscillations. Evaporation of this water alters the bubble period, oscillation amplitude and migration rate. These effects are particularly important in subscale testing. Hydrodynamic and/or diffusive instabilities of the interface are observed during some phases of the motion. Evaporative instability could be the rate–determining process that limits mass transfer. Taylor instability during the bubble collapse phase could limit the collapse velocities and the strength of the associated jets produced near boundaries. Our present understanding is summarized and future research areas are identified.

Introduction

A conventional underwater explosion creates a bubble of hot product gases (a mixture of water, carbon dioxide, carbon monoxide, nitrogen, hydrogen, and sometimes solid carbon or metal oxides) at high temperature (2000–4500 K) and pressure (150–400 kbar). The exact composition and thermodynamic state of the products depend on the type of explosive and it's elemental composition. The bubble of products rapidly expands, producing a shock wave in the surrounding water. The shock wave decays as it moves outward and the bubble oscillates and migrates upward (Fig. 1). In addition to the initial shock wave, a sequence of smaller pressure waves or "bubble pulses" are produced at the minimum radius of each bubble oscillation cycle.

The **interface** is the surface or more generally, region, between the explosive products and surrounding water. The interfacial region serves to couple the motion of the product gases to the surrounding water. In turn, the motion and thermodynamic state of the fluid adjacent to the interface determine the energy and mass transfer processes

across the interfacial region. It is this nonlinear coupling that is really being referred to when we talk of interface dynamics. The subject of the present report is the effects of interface dynamics on all the phenomena associated with underwater explosions. The phenomena affected include: shock pressure and decay rate; bubble oscillation period and amplitude; bubble pulse magnitude and shape; bubble migration rate; bubble-structure interaction, i.e., the formation of jets during the collapse phase.

The physical processes that are important to the present discussion are indicated on the idealized space–time diagram of Fig. 2. On this graph are shown the trajectories of the detonation, interface, shock wave in the water, pressure waves within the products, and also the bubble overexpansion, collapse, and rebound. The bubble oscillation period has purposely been made unrealistically small in order to show all these features on the same plot. The processes indicated are: A – detonation propagation; B – detonation-water interaction; C – gasdynamics within the bubble; D – acoustic wave interaction with the interface; E – disturbance propagation up to the shock; F – shock compression of the water; G – evaporation of the water at the interface; H – isentropic expansion of the products; I – interface instability near collapse; J – geometrical vs nonlinear effects in bubble pulse propagation. In the three sections that follow: Detonation Wave Interaction; Mass Transfer; and Instabilities, these physical processes are discussed with a particular emphasis on the relationships to the interfacial region and dynamics.

In writing the present review, three sources of information were used: the classical references[1,2] from World War II; papers published in journals and symposia; and contractor and government laboratory reports. It is clear that the most widely known reference, R. H. Cole's book **Underwater Explosions**,[1] which pays scant attention to interface issues, is completely out of date. Unfortunately, this is the only readily available comprehensive compilation of information. A new primer and reference book is sorely needed to help newcomers to this field.

Detonation Wave Interaction

The physical process which dominates the initial phase of the explosion is the propagation of the detonation wave through the explosive and the interaction with the surrounding water. Numerical computations of this process show that this interaction generates a complex system of waves propagating within the products, partially reflecting from the interface and catching up with the shock wave. The results of Sternberg and Walker[4] for a Pentolite sphere are shown in Fig. 3.

When the detonation reaches the edge of the explosive, a shock wave is propagated outward into the water and an expansion wave is usually propagated back into the explosive products. Both waves then interact with the expansion or "Taylor" wave that follows the detonation. However, near the instant of interaction the process can be idealized as the production of two simple waves at a planar surface, shown in Fig. 4. The pressure at the interface immediately following interaction can be determined

by matching pressure and velocity at the contact surface (the water-product interface); this matching process is shown graphically in Fig. 5.

To carry out this computation, we must know the Chapman-Jouguet state of the explosive, the equation of state of water and also the explosive products. The TIGER computer code[5] was used with the BKW equation of state (with the LLNL recalibrated constants[6]) and standard thermochemical parameters.[7] The hugoniot for water was taken from the experimental data and analysis reported by Rice and Walsh[8], Gurtman et al.[9], and Steinberg[10]. The explosive product isentropes were either obtained from the JWL equation of state[7] or computed using TIGER and the BKW equation of state.

The results for 5 explosives: HMX, Pentolite, H-6, TNT, and NM are given in Table 1 and Fig. 6. All these materials *except* H-6 are simple CHNO compounds that behave as ideal explosives in kilogram quantities, i.e., they have short reaction zones, small failure diameters, detonation velocities independent of size and good agreement between computed and measured properties. H-6 is a mixture of CHNO explosives and aluminum (in particulate form) and is more typical of explosives used in modern underwater applications; it exhibits nonideal behavior: a strong size dependence of measured properties. The interface pressures range from a high value of 230 kbar for HMX down to 121 kbar for NM; the CJ state for NM is so close to the water hugoniot that only a small expansion wave is reflected back into the products.

This computation illustrates one difficulty in obtaining high water shock pressures and associated high strain rates on adjacent targets. A substantial amount of the high pressure generated by detonating RDX is reflected back into the products due to the impedance mismatch with the water. Furthermore, the remaining energy in the high pressure shock is rapidly dissipated due to the irreversible nature of the shock wave propagation. The difference between isentropic compression and shock compression as represented in pressure–volume coordinates (Fig. 7) is due to the increase in entropy across the shock wave. As the shock pressure is released by the essentially isentropic wave system following behind, the water pressure returns to ambient but the temperature and specific volume (see Fig. 7) are higher due to the energy deposited by the shock wave. This shock heating has three effects: the shock wave in the water decays rapidly after leaving the interface; a layer of superheated water is created next to the bubble; and less energy remains in the water–bubble system to drive the oscillation process. The heating effect is confined to a thin layer due to the rapid attenuation by geometrical spreading, the interaction with transmitted Taylor wave, and the increase of the entropy jump with increasing shock strength.

The entropy increase across the shock wave can be computed from the experimental hugoniot and simple thermodynamic relations as described in Ref. 8. If we neglect diffusive thermal transport processes within the water , a reliable approximation in most shock propagation problems, the entropy change in a fluid element depends only on the strength of the shock wave at the time it passed through that location. This function, entropy jump vs shock pressure, is shown in Fig. 8. These entropy changes will be used, in conjunction with a temperature-entropy phase diagram of water, to

examine in the next section the issue of superheating and evaporation.

The effect of the initial shock pressure and fraction of the explosive energy dissipated by the shock has been parametrically studied by Sternberg and Hurwitz[11]. They computed energy budgets (shown in Fig. 9) as a function of shock position for 4 explosives. The highest shock pressure and largest dissipation is generated by detonating PBX9404 (the principle ingredient is HMX); over 50% of the original energy has been dissipated when the shock has reached 30 R_o, where R_o is the initial charge radius. The Pentolite has a CJ and initial interface pressure that is two–thirds that of PBX9404; 40% of the initial energy has been dissipated at 30 R_o. A constant–volume explosion of high–density (1.65 g/cm^3) Pentolite produces an interface pressure of 30 kbars and results in 30% of the original energy being dissipated at 30 R_o. The constant volume explosion of low–density (0.4125 g/cm^3) Pentolite produces an interface pressure of 6 kbars and results in less than 5% of the energy being dissipated by 30 R_o.

How does this wide range of interaction pressures and dissipation rates affect the pressure wave at some distance from the explosive? In applications and experimental measurements, it is not the interface pressure that is significant but the pressure at some distance away from the explosive. Weapon systems operate with a range of standoff distances from the target; pressure and shock trajectory measurements are performed in the water surrounding the charge. The shock pressure at a given location is the result of several factors: the initial interface pressure; decay due to the geometrical increase in shock front area; and the integrated effects of the interface motion producing acoustic signals that propagate from the interface to the shock. These signals are propagated along characteristics as shown in Fig. 10.

The net result of these processes on near and farfield pressure are shown in the pressure vs. distance diagram of Fig. 11, taken from Sternberg and Hurwitz. The four cases shown correspond to those of Fig. 9 and the size of the individual charges have been adjusted so that the total energy release is the same in all cases. In the near field (at distances of 1-4 charge radii), the interface pressure substantially influences the shock pressures; lower interface pressures result in lower shock pressures at the same scaled distance.

However, as the distance from the charge is increased, the lower interface pressure is compensated for by lower dissipation and a lower shock decay rate. This lower decay rate is due to the interface deceleration being lower in the constant–volume and low–density explosions than in the high-density detonation cases. The net result is that the three cases with similar initial explosive density yield essentially identical pressures at the same scaled distance from the charge, beyond 5–10 charge radii. This result is the basis of the standard explosive scaling rules,[3,12] which holds that for equivalent energy releases, the far field pressures are the same at equal scaled distances. This scaling appears to hold for a variety of atmospheres and explosives, including air,[11,12] there is however, an initial density effect that is imperfectly understood. Very low density explosives can show significant departures from the standard scaling rules. This has been observed[13,14] in soviet tests of underwater gaseous detonations and can be seen in

the low density Pentolite explosion results shown in Fig. 11.

Clearly, a low *brisance* (small CJ pressure) explosive is better for transferring kinetic energy to the water and obtaining large amplitude bubble oscillations. This advantage is obtained at the expense of lowering the initial shock pressure. Apparently the only manner to obtain high strain rates is through high initial shock pressure and concomitant dissipation. The optimum tradeoff between high initial shock pressure and high final bubble energy must be determined by considering damage mechanisms and the particular weapon application. The results shown in Fig. 11 suggest that the standoff distance is a key parameter in these considerations.

In addition to the simple thermodynamic and hydrodynamic factors mentioned above, there are other issues that must be considered when examining real systems. Among these are: the nonideal nature of many explosives, particularly aluminized materials used in modern underwater weapon systems; influence of an extended reaction zone structure behind the detonation front; multi-dimensional nature of charge and detonation front geometry; curvature effects on detonation propagation; the nonideal character of the interface in a cased charge; attenuation of the shock while propagating through the case. Two of these issues: the influence of adding aluminum to the explosive and the effect of a metal case, are discussed next.

The addition of powdered or flake aluminum (micron-size particles) to a conventional explosive is found to significantly improve the performance in underwater applications. The equivalent amount of energy, as determined by intermediate-field (5–10 R_o) shock pressure measurements and bubble oscillation period determinations, is an increasing function of aluminum concentration (see Fig. 12) up to an aluminum/oxygen molar ratio of 0.4. A substantial fraction of this gain is just due to the better energetics of aluminum as a fuel rather than carbon.

Computations and measurements[7] indicate that the heat of detonation (the energy available per mass of explosive) is an increasing function of the aluminum content. As shown in Table 2, the heat of detonation of RDX is 6.15 MJ/kg; addition of 30 wt % Al increases this to 10.12 – a factor of 1.64. Fig. 12 indicates a bubble energy increase of 1.9 over pure RDX and an equal strength shock wave. However, it cannot just be energetics alone since the energy distribution is shifting from the shock wave to the bubble with increasing aluminum concentration.

Some of this shift is due to the decrease in Chapman-Jouguet pressures and therefore, lower interface pressures and shock dissipation, with an increasing fraction of aluminum. Calculated interface conditions for some RDX/Al explosive mixtures are shown in Fig. 13 and given in Table 2. These are idealized computations in which the aluminum is quickly burned to Al_2O_3(s) and the free carbon rapidly coagulates into a solid graphitic form. The formation of C(s) and Al_2O_3(s) are interrelated since the product composition shifts

$$CO + CO_2 + 2Al \rightarrow 2C(s) + Al_2O_3$$

to these condensed species with increasing amounts of initial aluminum.

The ideal interaction pressures are lowered but not enough to provide the gain in bubble oscillation energy shown in Fig. 12. This implies that the nonideal nature of these explosives is responsible for the remaining shift in energy distribution. The obvious problem with the ideal theory is the assumption of the rapid formation of both Al_2O_3(s) and graphitic carbon clusters within a short reaction zone. These processes both involve heterogeneous reactions and species diffusion to and from particles of up to micron size; the slowness of diffusive processes in comparison to unimolecular or bimolecular reactions suggests a two–stage reaction zone.

In the first stage, lasting nanoseconds, molecular products such as H_2O, CO, CO_2, and H_2 are produced; in the second, lasting microseconds,[13] the Al_2O_3 and C atoms coagulate into clusters. This two–stage process and the introduction of a long reaction time scale will cause the detonation development to steady state to be delayed and the ideal conditions will be achieved only after a long buildup time in an exceedingly large charge. During the buildup period, the detonation and interface pressures will be lower than predicted by the ideal theory and the long–time–scale reactions will contribute to the bubble energy rather than the shock.

The maximum reductions in detonation and interface pressure can be estimated by performing the detonation thermochemical computations without any solid product formation. For 15 wt % Al in RDX/Al explosive, the detonation pressure is reduced from 331 to 305 kbar and the interface pressure from 200 to 187 kbar. For 30 wt % Al in RDX/Al explosive, the detonation pressure is reduced from 267 to 171 kbar, the interface pressure from 150 to 96 kbar. There is also evidence[14] that the microstructure of these heterogeneous materials can produce comparable nonideal behavior that results in substantially lower detonation front pressures at nearly ideal values of the detonation velocity.

Weapon systems and many experiments use a metal case to contain the explosive. This case will interact with the detonation wave (Fig. 14a) and produce nonideal interface conditions and an extended multiphase region instead of a sharp discontinuity. Impedance mismatches at the explosive–case and case–water interface will produce multiple reflections (Fig. 14b) and an interface pressure lower than ideal. In addition, the expansion wave following the detonation will attenuate the initial shock as it traverses the case material, this will also reduce the interface and water shock pressure as shown in Fig. 15a. The high strains and strain rates induced in the case by the explosion will cause fracture of the case and the shock heated fragments will be dispersed into the surrounding water and products. The mixing action of the dispersal process and the heat transfer from the case fragments will result in the creation of the multiphase interface region shown in Fig. 15b. Such an extended region will behave very differently than the ideal interfaces considered so far.

Mass Transfer

Mass transfer between the explosion products and surrounding liquid water can occur through several mechanisms: evaporation, condensation, dissolution of product gases into the water, explosive boiling of superheated liquids, and direct entrainment of gases into the liquid water. Two causes of mass transfer will be examined in this section; first is the rapid evaporation or explosive boiling of the shock–heated water located within the entropy layer next to the bubble surface; second is the evaporation that occurs when the overshoot in bubble size results in a reduction of the partial pressure of water in the explosion products below the equilibrium vapor pressure of the liquid on the bubble surface.

The magnitude of the effects associated with these processes depends very strongly on the ambient conditions (water temperature and pressure). Evaporation effects appear to be much more significant for scale modeling done at reduced pressure than for deep ocean testing. Parameters associated with bubble motion are most likely to be affected by evaporation. Observations of bubble oscillation period, oscillation amplitude, bubble migration rates, and bubble interaction with structures all show a pronounced effect of ambient conditions in subscale testing and can cause failures in similitude.

As discussed in the previous section, a layer of high–entropy water is created next to the bubble due to shock heating (see Fig. 16). This layer becomes superheated when the interface pressure decreases after the shock has propagated away and the bubble begins to expand. The superheated water can rapidly evaporate into the bubble, mixing with the existing products of the explosion. The amount of water that is superheated depends on several factors: the initial strength of the shock wave; the rate of decay; and the ambient pressure. The relationship between these factors can be illustrated on a temperature–entropy diagram (Fig. 17) for water.

When the shock wave overtakes a fluid element, the fluid state will jump up to a point on the indicated hugoniot of Fig. 17. Following the passage of the shock, the state of the fluid will move from the shock adiabat vertically downwards along an isentrope, examples of which are shown on Fig. 17. As the shock moves away from the bubble and the strength decays, the entropy decreases back toward ambient. When the fluid state passes through the coexistence curve (denoted σ on Fig. 17), the water becomes superheated. At a given pressure, this occurs first for the highest entropy states adjacent to the interface. The entropy jump for these states (ΔS) and the pressure (P_σ) at which the coexistence curve is encountered, is given in Tables 1 and 2 for each of the explosives discussed in the previous section.

The shocked interface coexistence pressures range from a high of 140 bars for HMX to 8 bars for NM. The actual minimum pressure achieved at the interface is determined by the ambient pressure and the bubble dynamics. The ambient pressure is usually expressed in terms of the equivalent depth of the water (taking into account reduced surface pressure for subscale modeling). For reference, a depth of 100 meters in the ocean corresponds to 11 bars ambient pressure, the critical pressure of water, 220

bars, is reached at a depth of 1.3 miles. Due to the overshoot of equilibrium during bubble oscillations, the minimum interface pressure (at maximum bubble radius) can be as much as 10-50 times below ambient. Therefore, for almost all of the explosives mentioned in Tables 1 and 2, some water near the interface will become superheated and evaporates if the explosion occurs at a depth of 100 meters or less.

How much of the water in the entropy layer will actually change phase? Numerical computations are required for each type of explosive in order to predict the entropy distribution and interface pressure histories needed to answer this question. Sternberg and Walker[4] found that the water out to a radius of $1.3R_o$ could be evaporated in a shallow (ambient pressure of 1 bar) pentolite detonation (they did not actually include this effect in their computations). This represents a volume of water that is 1.2 times the original explosive volume or a mass of water that is 0.7 of the original explosive mass. The coexistence curve is encountered by the interface fluid fairly early in the bubble expansion process, at an interface location of $3.9R_o$; for comparison, the equilibrium radius is at $20R_o$ and the maximum radius is at $32R_o$.

An increase of 70% in the mass of the bubble is very substantial but represents a change of only 20% in the equivalent bubble radius. This figure is an upper bound computed for a ideal detonation in an uncased charge. Nonideal detonation propagation and case effects will both tend to lower the shock and interface pressures, decreasing the amount of water vaporized. This example is for an explosive with a value of 40 bars for P_σ, which is in the middle of the range for the explosives examined above. The amount vaporized also decreases dramatically with increasing depth. At a depth of 100 m, only fluid that has been shocked to greater than 100 kbar will evaporate – this represents a negligible addition to the mass of the bubble. We conclude that this effect is most important for high brisance explosives at small depths.

In the discussion above, it has been assumed that any water that is superheated will evaporate. However, the evaporation process may be limited by the rate at which water molecules are ejected from the liquid and transported away from the interface. If the evaporation rate is unable to keep up with the rate at which fluid is being superheated, then a nonequilibrium situation is created at the interface. A layer of metastable (superheated) water will be created next to the surface which, if sufficiently superheated, could rapidly (explosively) evaporate. This situation is plausible because the rate of superheating and the rate of evaporation are determined by completely different mechanisms. The existence of superheated liquids and the process of explosive evaporation have also been extensively documented.[17]

The intrinsic rate at which molecules are ejected from the liquid into the vapor is controlled by the molecular dynamics of the superheated liquid[18] and the gas kinetics of the Knudsen layer[19] between vapor and the liquid, Fig. 18a. In cases where the evaporation rate is low and the liquid at the interface is close to equilibrium, these processes act to keep the partial pressure of evaporated liquid close to it's equilibrium value. The net rate of evaporation is then determined by the coupled problem of transporting vapor away from the interface and energy towards it, shown in Fig. 18b.

If diffusion is the only transport mechanism, bubbles in a uniformly superheated liquid will grow in an unsteady manner, the radius increasing with $\sqrt{t}$ and the mass flux inversely proportional to $\sqrt{t}$.[20] This is the process that controls the growth of bubbles in ordinary boiling. A similar process will control the evaporation rate of a near-equilibrium bubble surface created by a deep underwater explosion or a shallow low–brisance explosive. The thermal and mass transport processes occurring in the boundary layers adjacent to the interface will determine the evaporation rates and ultimately, the net effect of evaporation on the bubble motion.

Numerical techniques developed for unsteady laminar mass–transfer boundary–layer problems in chemical processing, heat transfer, and combustion applications could be applied to solve this problem. A number of methods exist[20] for modeling bubble growth under conditions of ordinary boiling that could be extended to treat the explosion bubble problem. Some features that are particular to the explosion bubble are: gas and liquid motion induced by the explosion; nonuniform superheating of the liquid; time dependent gas and liquid thermodynamic states; radiant heat transfer from the explosion products; and real fluid (compressibility) effects in the gas.

A much more difficult problem is to treat the case of an interface far from equilibrium. The mass flux can approach the kinetic theory limit of the one-way molecular flux $n\bar{c}/4$. The proper interface boundary conditions are poorly understood; the high mass fluxes through the phase interface can create instabilities of the interface; liquid droplets may be ejected from the surface along with vapor, creating a multiphase flow within the bubble. These effects have been observed in experiments[21,22] designed to examine the phenomenon of rapid evaporation of superheated liquids. There has been some consideration of nonequilibrium effects in modeling evaporation[23] or condensation[24] during bubble or cavity motion. However, a comprehensive model for the rapid evaporation of superheated liquids that accounts for all these observations and postulated effects is yet to be developed.

As the evaporation proceeds, a layer of evaporated vapor will build up next to the interface. This water vapor is transported away from the interface by diffusion and the convective motion of the explosion products. Deep explosions result in spherical bubbles during the initial expansion phase and only radial motion of the products occurs; diffusion is the only means of transporting vapor away from the interface in these cases. Bubbles created by shallow explosions quickly become deformed due to the large gradient in pressure and influence of the nearby boundaries (water surface and bottom). In these cases, significant product motion transverse to the interface and an overall internal circulation within the bubble may occur. If the Reynolds number is large enough, the flow will be turbulent, greatly enhancing the mixing of evaporated water vapor with the explosion products. While such effects have been considered for conditions encountered in ordinary boiling, there have been no applications to the mass transport problem for explosion bubbles.

One cause of evaporation is the superheated water originating in the entropy layer. Another cause of evaporation is the reduction in pressure within the gas bubble when

the equilibrium position is overshot during the oscillation cycle. This behavior is shown in Fig. 19 for an explosion of 250 g of tetryl at a depth of 300 ft (from Cole, Ref. 1). The experimental measurements of bubble radius vs. time were used to infer the pressure, assuming uniform conditions within the bubble and isentropic changes in state (JWL equation of state). In this case, the pressure minimum of 0.24 bar is much less than the ambient pressure of 10.4 bar but still greater than the equilibrium vapor pressure of 0.035 bar for 300 K water.

Therefore, at this depth no evaporation will occur due to the pressure undershoot. At lower depths, the minimum pressures will be even lower and evaporation will commence if the partial pressure of water in the explosive products (water is typically 20–30 mol % of the products for CHNO explosives) drops below the saturation pressure at the ambient temperature. In effect, the liquid water at the interface becomes superheated when this happens and evaporation occurs as the system attempts to restore equilibrium. Increasing the ambient temperature increases the saturation pressure and the likelihood of evaporation. This effect is particularly significant in scale model testing.

Scale model testing of underwater explosives is designed to preserve geometric and dynamic similarity of the bubble motion. Geometric scaling means preserving the ratio R_{max}/d of bubble maximum size R_{max} to depth d; the amplitude of the bubble oscillation R_{max}/R_{min}; and the ratio of structure to bubble size. Dynamic scaling means preserving the ratio of inertia to buoyancy forces, the Froude number $Fr = U^2/gL$, where U is a characteristic velocity and L a characteristic length. For a length scale, the bubble maximum radius is used $L \sim R_{max}$; the velocity scale is $U \sim R_{max}/T$ where T is the bubble oscillation period. In terms of the bubble parameters, a constant Froude number is equivalent to a scale-invariant parameter $F = T^2/R_{max}$. The parameters T and R_{max} now have to be determined as functions of initial and ambient conditions using the dynamics of the bubble–water system.

The one-dimensional dynamics of a gas bubble within an liquid is, in the simplest approximation, controlled by a nonlinear second-order differential equation[20]

$$R\frac{d^2R}{dt^2} + \frac{3}{2}\left(\frac{dR}{dt}\right)^2 = \frac{P(V) - P_\infty}{\rho_o}$$

where

$$P(V) = P_o\left(\frac{V_o}{V}\right)^\gamma, \quad \gamma \approx 1.2, \quad V = \frac{4}{3}\pi R^3$$

known as the Rayleigh or bubble equation. The oscillatory solutions to this equation and the various improved versions can be used to predict the purely radial motion of a deep explosion. The initial conditions to this equation are determined by the total amount of energy in the bubble-water system E_b, which is approximately 40% of the available energy ΔH_{det} in the explosive (for conventional CHNO materials).

From the solutions to this equation, simple scaling relations can be established for the period T, maximum radius R_{max}, and the amplitude of oscillation R_{max}/R_{min}

$$T \sim \rho_o^{1/4} \frac{E_b^{1/3}}{P_o^{5/6}}, \quad R_{max} \sim (E_b/P_o)^{1/3}, \quad R_{max}/R_{min} \sim P_o^{-1/3}$$

If the geometric scaling factor is λ between two configurations (labeled 1 and 2) , then geometric similarity requires that $\lambda = R_{max,2}/R_{max,1} = d_2/d_1$. Dynamic similarity requires that $F_1 = F_2$. These similarity conditions then reduce to the following scaling relations for pressure depth $Z = d + P_s/\rho_o g$ and bubble energy:

$$Z_2 = \lambda Z_1, \qquad E_{b,2} = \lambda^4 E_{b,1}$$

The linear reduction in pressure depth Z and physical depth d combined imply a corresponding reduction in the surface pressure P_s. This is the reason scale modeling is done in vacuum tanks at reduced surface pressures.

Scale model testing of the interaction of bubbles with structures was performed at NSWC[25,26,27] in a vacuum tank facility using very small charges (0.2 g) of lead azide located at a depth of 2 ft, the total tank depth was 6 ft. The principal observations were motion studies using movies of bubbles. The parameters varied included surface pressure (.15 – 1 bar) and ambient temperature (36 – 100 °F). After correction for a substantial effect of the nearby surfaces, significant departures from the standard scaling laws for bubble period and maximum amplitude were observed.

In terms of charge mass W and pressure depth Z, the scaling law for period (Willis formula[3]) is

$$T = K \frac{W^{1/3}}{Z^{5/6}}$$

where for deep charges, $K_\infty = 2.11$ (SI units) for TNT and the correction[3] for a free surface is

$$K = K_\infty (1 - 0.214 R_{max}/d)$$

The scaling law for maximum radius[3] is

$$R_{max} = J \frac{W^{1/3}}{Z^{1/3}}$$

where the constant is $J_\infty = 3.5$ (SI units) for TNT. The variation of the measured period and amplitude coefficients K and J from the standard values is shown in Figs. 20 and 21. Note that period constant is almost double the standard value at the smallest pressure depths and the highest ambient temperatures. Examination of photographs of the bubble surface reveals a very smooth bubble surface for the 36 °F tests and a rough appearance for 100 °F tests. Both the systematic variation in period constants and the bubble appearance indicate the occurrence of evaporation and the influence of mass transfer on the bubble motion.

Instabilities

There are two types of instabilities that are significant to the interface development and can influence bubble motion. Hydrodynamic instabilities such as Rayleigh-Taylor or Kelvin-Helmholtz mechanisms rely on feedback between the interface distortion and the induced fluid motion. Evaporative instabilities such as the Landau-Darrieus mechanism are more complex and involve feedback between vorticity production, evaporative mass flux, vapor pressure, liquid temperature distribution, and interface distortion. Hydrodynamic instabilities are most significant near the end of the first bubble oscillation cycle, when the interface velocities and accelerations are highest. Evaporative instabilities only operate when there are large evaporative mass fluxes: this is possible whenever the liquid is strongly superheated by either the entropy layer or pressure undershoot mechanisms.

The Rayleigh–Taylor mechanism produces a dramatic and permanent effect when the bubble passes through the end of the first oscillation cycle. Photographs of the bubble (see Refs. 21 and 22) after this time show a surface that is wrinkled and bulging with the disturbances characteristic of the nonlinear "bubble and spike" configuration of the developed instability. These extreme distortions in the interface shape result in the interpenetration of the water and explosion products; this is the direct entrainment mixing mechanism mentioned above. Under conditions of constant acceleration, the mixed region grows quadratically[28] with time. In the explosion bubble, accelerations are time dependent and scaling rules for the extent of the mixed region have not yet been developed. The bubbles of product gas protruding into the water eventually break off and separate from the main bubble. In this manner, the bubble is broken down into a mixed region and isolated smaller bubbles over a number of oscillation cycles.

A planar interface is Taylor–unstable if the accelerations are directed from the light fluid into the dense fluid. This occurs in an explosion bubble when the gas is being compressed and decelerates the surrounding liquid water. Therefore we expect that a detailed stability analysis for a spherical interface (bubble surface) will reach that conclusion. A rigorous criterion for instability can be obtained by analyzing the linear stability of the Rayleigh equation to three-dimensional distortions of the bubble surface. This results in a linear, second-order equation (with time-dependent coefficients) for the disturbance amplitude.

Birkhoff[29] first completely analyzed the stability conditions for the spherical surface; the application to explosion bubbles is discussed in Ref. 21. Referring to the bubble oscillation cycle shown in Fig. 22, there are three cases depending on the signs of the radial velocities and acceleration. Case A, collapsing and decelerating – potentially unstable, with algebraic growth of oscillatory disturbances; Case B: collapsing or expanding, accelerating: potentially unstable with monotonic, exponential growth; Case C: expanding and decelerating – absolutely stable. The case of greatest interest is B, a catastrophic instability that is possible whenever the radial accelerations are large and positive. This is equivalent to the Taylor instability criterion for planar interfaces.

The region of the bubble oscillation cycle in which this instability is possible is shown in Fig. 22. Note that this instability will not occur for all bubbles, but only if the oscillation amplitude is large enough.

If the bubble is unstable, there are a range of unstable wavelengths (discrete mode numbers) which have positive growth rates when the accelerations are large and positive. A maximum wavelength is fixed by the size of the bubble; a minimum wavelength is determined by the effects of surface tension. Within this range, there is a most unstable wavelength that will be preferentially amplified. This wavenumber selection process will determine the length scale for the subsequent nonlinear development of the instability. This has been demonstrated for very low energy, small–scale explosions by photographic measurements[21] of the characteristic disturbance scale immediately following the minimum radius point of the first oscillation cycle. The disturbance amplitude is usually so large after this time that the linear theory is no longer applicable and the nonlinear evolution of the interface must be considered.

What is the impact of this instability process on the overall bubble dynamics? Apparently there has been little systematic investigation of this effect. Cole[1] reports some bubble pulse pressure measurements and notes a lack of agreement with the computations available at that time. We can safely speculate that the interface instability will be a mechanism for removing energy from the bubble and should lessen the severity of the collapse process. In the case of collapse near boundaries, jet formation may be inhibited and the collapse velocities decreased. The effectiveness of the jet impingement as a damage mechanism will be diminished.

A different form of the Rayleigh–Taylor instability may be operative near the beginning of the explosion process but is not observed with conventional underwater explosives. A impulsive destabilizing acceleration is produced when the detonation wave breaks out of the explosive and the transmitted shock enters the water. This impulsive version of the Rayleigh–Taylor mechanism is known as the Richtmyer–Meshkov instability, a subject of current numerical[30] and experimental[31] investigation.

Unlike continuous acceleration, impulsive accelerations of any sign produce instability at an interface between fluids of different density and the disturbances initially grow linearly with time rather than exponentially. Apparently, the decelerating motion of the interface (which immediately follows the acceleration by the shock) stabilizes the Richtmyer–Meshkov mechanism. While no computations have been made to support this supposition, the physical mechanism is plausible. Is significant to note that experiments on extended interfaces[31], such as proposed above for cased explosives, show a dramatic slowing of the instability in comparison to sharp interfaces of the same density ratio.

Rapid evaporation instabilities are not as clearly understood as the Rayleigh–Taylor mechanism. There are numerous experimental observations of instability; particularly when the liquid is highly superheated.[21,22] These instabilities are very significant to determining the evaporation rate: unstable interfaces have effective evaporative mass fluxes that are a factor of 10^2 to 10^3 larger than predicted by the laminar diffusion–

limited theory. The observed instability onset and characteristic length scales appear to be consistent with the Landau-Darrieus mechanisms discussed in Refs. 21 and 22 but the details of the instability mechanisms remain to be clarified.

Theoretical research on evaporative instability has uncovered a variety of possible mechanisms involving the entire spectrum of transport processes and feedback mechanisms between the interface distortion and velocity, pressure, vorticity, and thermal fields in the liquid and vapor. The early studies of Miller[32] and Palmer[33] have been updated (and contradicted) by the more recent work of Prosperetti and Plesset[34] and Higuera.[35] A continuing experimental and theoretical effort will be required to unravel the complex nature of evaporative instability.

Summary

Three aspects of underwater explosions have been discussed: interaction of the detonation with the water; evaporation of water into the bubble of explosion products; and the instability of the interface between products and the surrounding water.

Upon reaching the edge of the explosive, the detonation wave produces a transmitted shock wave in the water and a reflected expansion in the explosive products. The transmitted shock provides the initial conditions for the shock propagation problem in the water. There is a tradeoff between producing a very strong shock which decays quickly and dissipates a large amount of the energy or using a lower pressure explosive with fewer losses and retaining more energy in the bubble-water system. The bubble motion generates acoustic signals which catch up to the shock and have a strong cumulative effect which is of even greater importance than the initial conditions in determining far–field shock pressures.

The optimum combination of near–field shock pressure and bubble energy needs systematic exploration. The effect of initial explosive density is not well understood. Nonideal effects in explosive propagation appear to have a significant role in shifting the energy budget from the shock to the bubble; further developments in detonation modeling are required to address this and the related issues of reaction zone structure, detonation wave instability and long–time–scale reactions.

Evaporation of water into the product bubble can be due to either the shock–generated entropy layer or pressure undershoot during the bubble oscillation cycle. Experimental observations in subscale testing verify that evaporation can significantly alter the bubble dynamics; particularly at small depths with high brisance charges. The evaporation rate will be determined by the coupled problems of mass and energy transport near the phase interface, the mass transport within the bubble by diffusion and convection, and the dynamics of superheated liquids. Existing data is difficult to interpret due to boundary effects. Numerical and analytical models of these processes need to be developed.

Instabilities of the interface are due to both hydrodynamic and evaporative mechanisms. Hydrodynamic instabilities such as the Rayleigh–Taylor mechanism are sig-

nificant near the minimum of the bubble oscillation cycle. Large deformations of the interface are produced at this point, destroying the symmetry of the collapse process and ultimately causing the fragmentation and destruction of the original bubble. Evaporative instabilities occur whenever the liquid is superheated sufficiently. These instabilities can greatly enhance the rate of mass transfer over the classical diffusion–limited values.

One of the most significant issues in modeling bubbles and predicting explosive performance is determining the composition and mass of the bubble as a function of time. What is the contribution of the entropy layer? How does the nonideal interface of real systems affect the transfer processes? What is the contribution of evaporation during pressure undershoot? Does evaporative instability play a role? It is important to develop complementary programs of analytical, numerical and experimental research to adequately answer these questions.

Acknowledgement

I would like to thank Georges Chahine (Tracor Hydronautics), Jules Enig (Enig Associates), Tom Farley, John Goertner (NSWC) and Paul Thibault (Combustion Dynamics) for their advice and references. John Goertner was particularly helpful in providing copies of his photographs and patiently explaining his experiments to me.

References

1. R. H. Cole **Underwater Explosions**, Dover, 1965.

2. **Underwater Explosion Research**, A Compendium of British and American Reports. Vol. 1 – The Shock Wave. Vol. II – The Gas Globe. Vol. III – The Damage Process. Office of Naval Research, Department of the Navy, 1950.

3. M. M. Swisdak (Editor) *Explosion Effects and Properties. Part II – Explosion Effects in Water*, NSWC/WOL TR 76-116, 1976.

4. H. M. Sternberg and W. A. Walker, "Calculated Flow and Energy Distribution Following Underwater Detonation of a Pentolite Sphere," *Phys. Fluids* **14**, 1869–1878, 1971.

5. M. Cowperthwaite and W. H. Zwisler *Volume IV, TIGER User's Guide*, SRI publication Z106, 1974.

6. M. Finger, E. Lee, F. H. Helm, B. Hayes, H. Hornig, R. McGuire, and M. Kahara "The Effect of Elemental Composition on the Detonation Behavior of Explosives," *6th Symp. (Intl.) on Detonation*, Office of Naval Research – Department of the Navy, ACR–221, 710–722, 1976.

7. B. M. Dobratz *LLNL Explosives Handbook – Properties of Explosives and Explosive Simulants*, UCRL–52997, March 1981.

8. M. H. Rice and J. M. Walsh "Equation of State of Water Compressed to 250 Kilobars," *J. Chem. Phys.* **26**, 824–830, 1957.

9. G. A. Gurtman, J. W. Kirsch, and C. R. Hastings "Analytical Equation of State for Water Compressed to 300 Kbar," *J. Appl. Phys.* **42**, 851–857, 1971.

10. D. J. Steinberg *Spherical Explosions and the Equation of State of Water*, LLNL Report UCID-20974, February 1987.

11. H. M. Sternberg and H. Hurwitz "Calculated Spherical Shock Waves Produced by Condensed Explosives in Air and Water" *6th Symp. (Intl.) Detonation*, Office of Naval Research - Department of the Navy ACR–221, 528–539, 1976.

12. W. E. Baker, P. A. Cox, P. S. Westine, J. J. Kulesz, R. A. Strehlow, **Explosive Hazards and Evaluation**, Elsevier, 1983.

13. S. M. Kogarko, O. E. Popov, and A. S. Novikov "Underwater Explosion of a Gas Mixture as a Source of Pressure Waves," *Combustion, Explosion, and Shock Waves* **11**, 648–654, 1975.

14. O. E. Popov and S. M. Kogarko "Comparative Characteristic of Pressure Waves in Underwater Explosions of Gaseous and Condensed High Explosives," *Combustion, Explosion, and Shock Waves* **13**, 791–794, 1977.

15. M. S. Shaw and J. D. Johnson, "Carbon Clustering in Detonations," *J. Appl. Phys.* **62**, 2080–2085, 1987.

16. C. L. Mader **Numerical Modeling of Detonations**, Univ. California Press, 1979.

17. V. P. Skripov **Metastable Liquids**, Wiley, 1974.

18. J. A. Blink and W. G. Hoover "Fragmentation of Suddenly Heated Liquids," *Phys. Rev. A* **32**, 1027, 1985.

19. D. A. Labuntsov and A. P. Kryukov "Analysis of Intensive Evaporation and Condensation," *Int. J. Heat Mass Transfer* **22**, 989-1002, 1979.

20. M. S. Plesset and A. Prosperetti "Bubble Dynamics and Cavitation," *Ann. Rev. Fluid Mech.* **9**, 145-185, 1977.

21. J. E. Shepherd and B. Sturtevant "Rapid Evaporation at the Superheat Limit," *J. Fluid Mech.* **121**, 379-402, 1982.

22. D. Frost and B. Sturtevant "Effects of Ambient Pressure on the Instability of a Liquid Boiling Explosively at the Superheat Limit," *J. Heat Transfer* **108**, 418, 1986.

23. W. J. Bornhorst and G. N. Hatsopoulos "Bubble-Growth Calculation without Neglect of Interfacial Discontinuties," *J. Appl. Mech.* **34**, 847-853, 1967.

24. S. Fujikawa and T. Akamatsu "Effects of the non-equilibrium condensation of vapour on the pressure wave produced by the collapse of a bubble in a liquid," *J. Fluid Mech.* **97**, 481-512, 1980.

25. H. G. Snay, J. F. Goertner, and R. S. Price *Small Scale Experiments to Determine the Motion of Explosion Gas Globes Towards Submarines*, NAVORD Report 2280, 1952.

26. J. F. Goertner *Vacuum Tank Studies of Gravity Migration of Underwater Explosion Bubbles*, NAVORD Report 3902, 1956.

27. J. F. Goertner, J. R. Hendrickson, R. G. Leamon *Model Studies of the Behavior of Underwater Explosion Bubbles in Contact with a Rigid Bottom*, NOLTR 68-207, 1969.

28. K. I. Read "Experimental Investigation of Turbulent Mixing by Rayleigh–Taylor Instability," *Physica* **12 d**, 45-58, 1984.

29. G. Birkhoff "Stability of Spherical Bubbles," *Q. Appl. Math.* **13**,451, 1956.

30. D. L. Youngs "Numerical Simulation of Turbulent Mixing by Rayleigh–Taylor Instability," *Physica* **12 d**, 32-44, 1984.

31. B. Sturtevant "Rayleigh–Taylor Instability in Compressible Fluids," *16th Intl. Symp. Shock Tubes and Waves*, Ed. H. Grönig, VCH, 89–100, 1988.

32. C. A. Miller "Stability of Moving Surfaces in Fluid Systems with Heat and Mass Transport – II. Combined effects of Transport and Density Differences Between Phases," *AIChE J.* **19**, 909, 1973.

33. H. J. Palmer "The Hydrodynamic Stability of Rapidly Evaporating Liquids at Reduced Pressure," *J. Fluid Mech.* **75**, 487, 1976.

34. A. Prosperetti and M. S. Plesset "The Stability of an Evaporating Interface," *Phys. Fluids* **27**, 1590–1602, 1984.

35. F. J. Higuera "The Hydrodynamic Stability of an Evaporating Liquid," preprint, 1987.

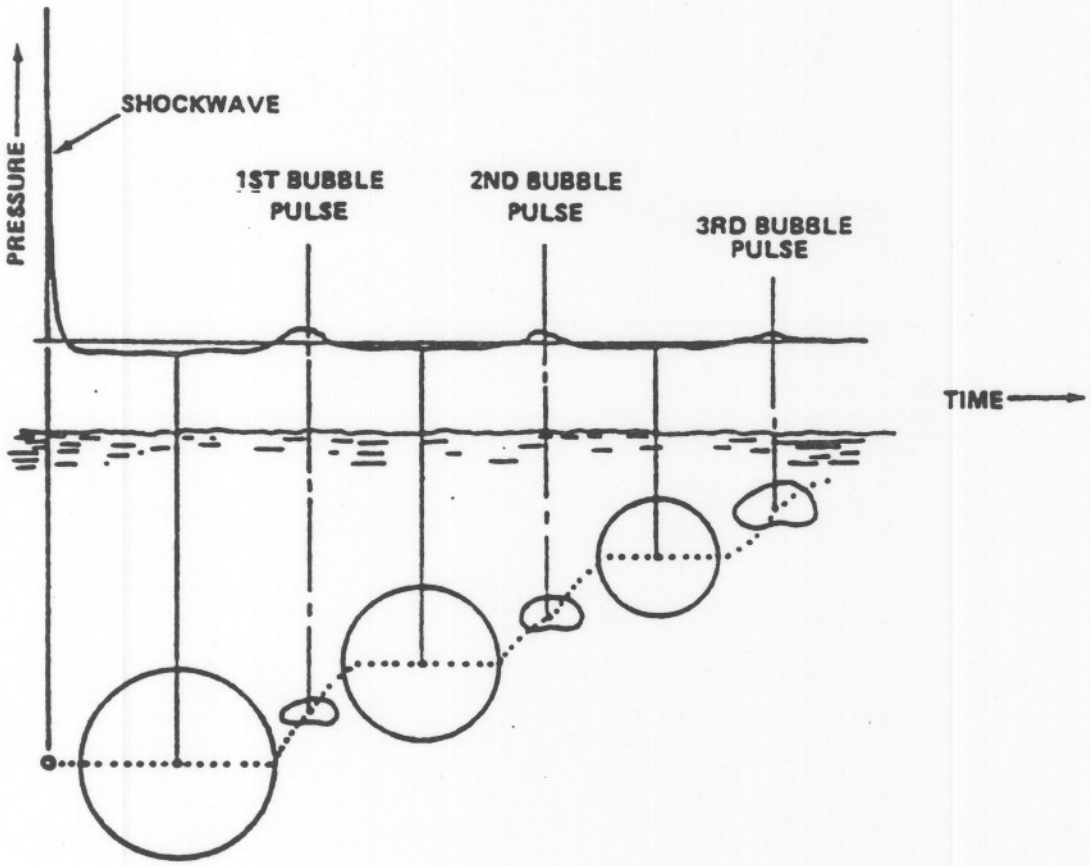

Figure 1. Schematic of an underwater explosion showing the principal phenomena. From Ref. 3.

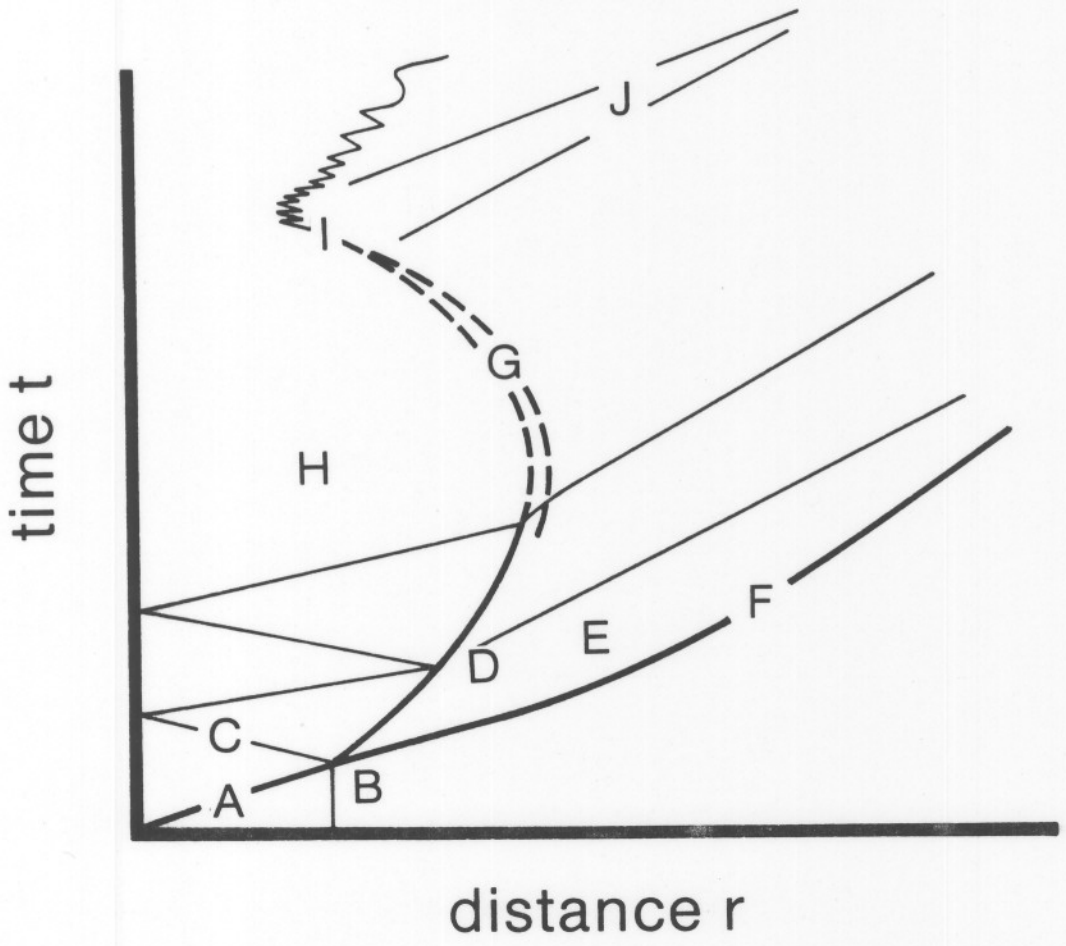

Figure 2. Schematic of interface and wave trajectories in an underwater explosion. The physical processes indicated are: A – detonation propagation; B – detonation-water interaction; C – gasdynamics within the bubble; D – acoustic wave interaction with the interface; E – disturbance propagation up to the shock; F – shock compression of the water; G – evaporation of the water at the interface; H – isentropic expansion of the products; I – interface instability near collapse; J – geometrical vs nonlinear effects in bubble pulse propagation.

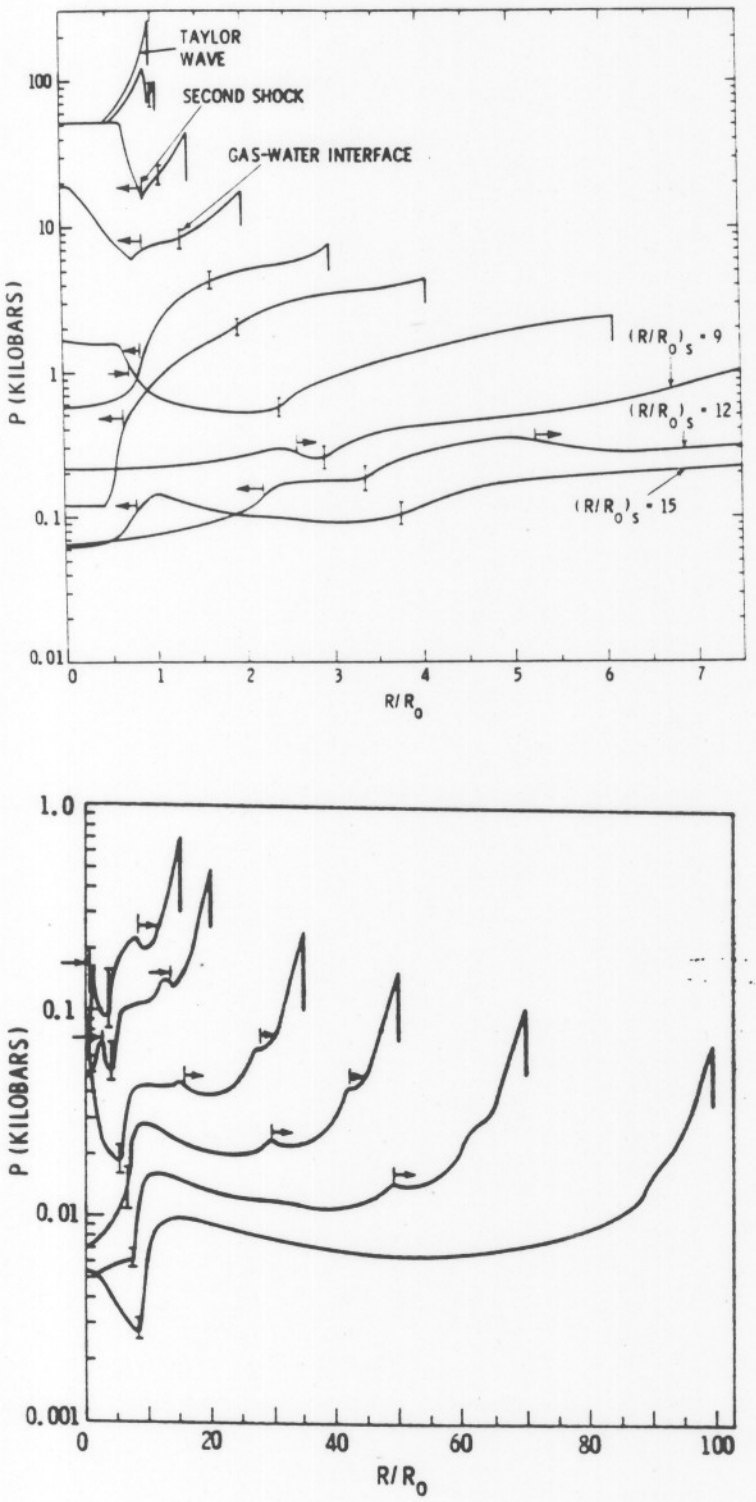

Figure 3. Pressure vs reduced distance for a spherical Pentolite detonation. From Sternberg and Walker, Ref. 4

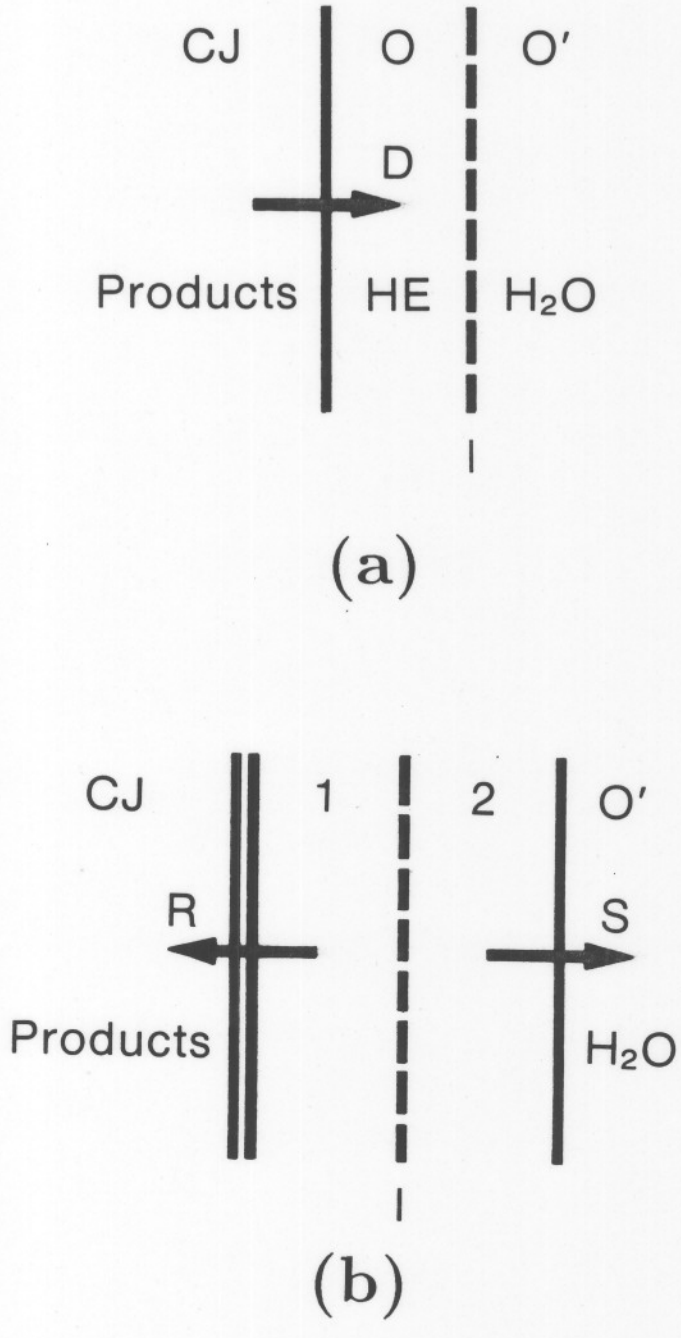

Figure 4. Idealized interaction between a detonation and the contact surface (water–explosive product interface). a) Before interaction, D – detonation, CJ - Chapman-Jouguet state. b) After interaction, S – shock in water, R – rarefaction or expansion wave in products.

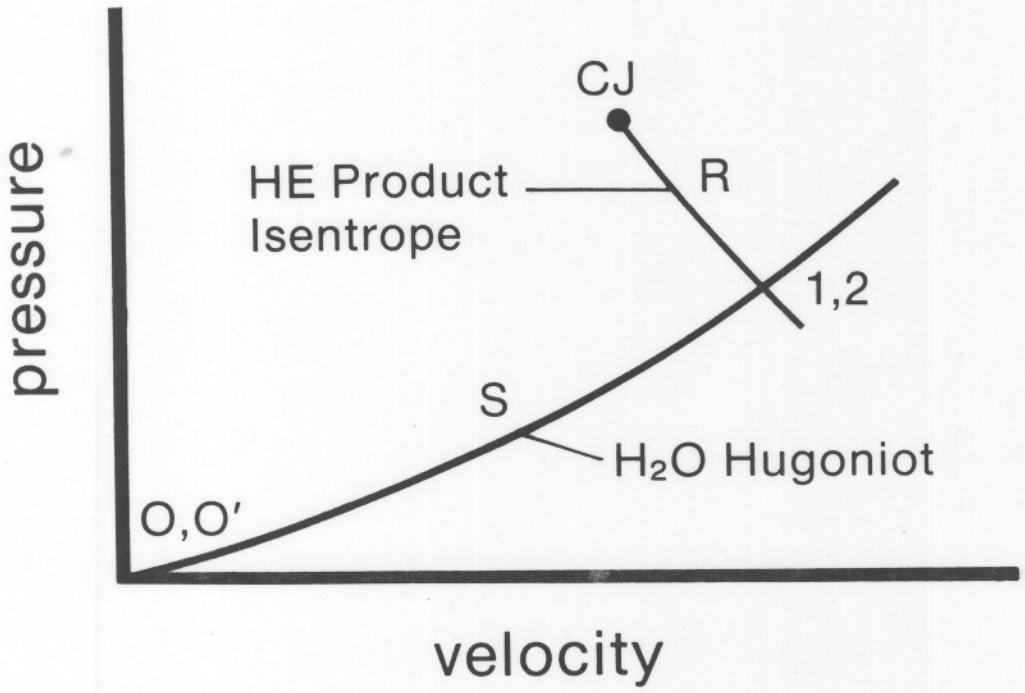

Figure 5. Pressure–velocity diagram for computing the interaction between a detonation and the contact surface (water–explosive product interface). O, Ó, initial states of explosive and water. CJ – Chapman-Jouguet state. S – shock in water. R – rarefaction or expansion wave in products.

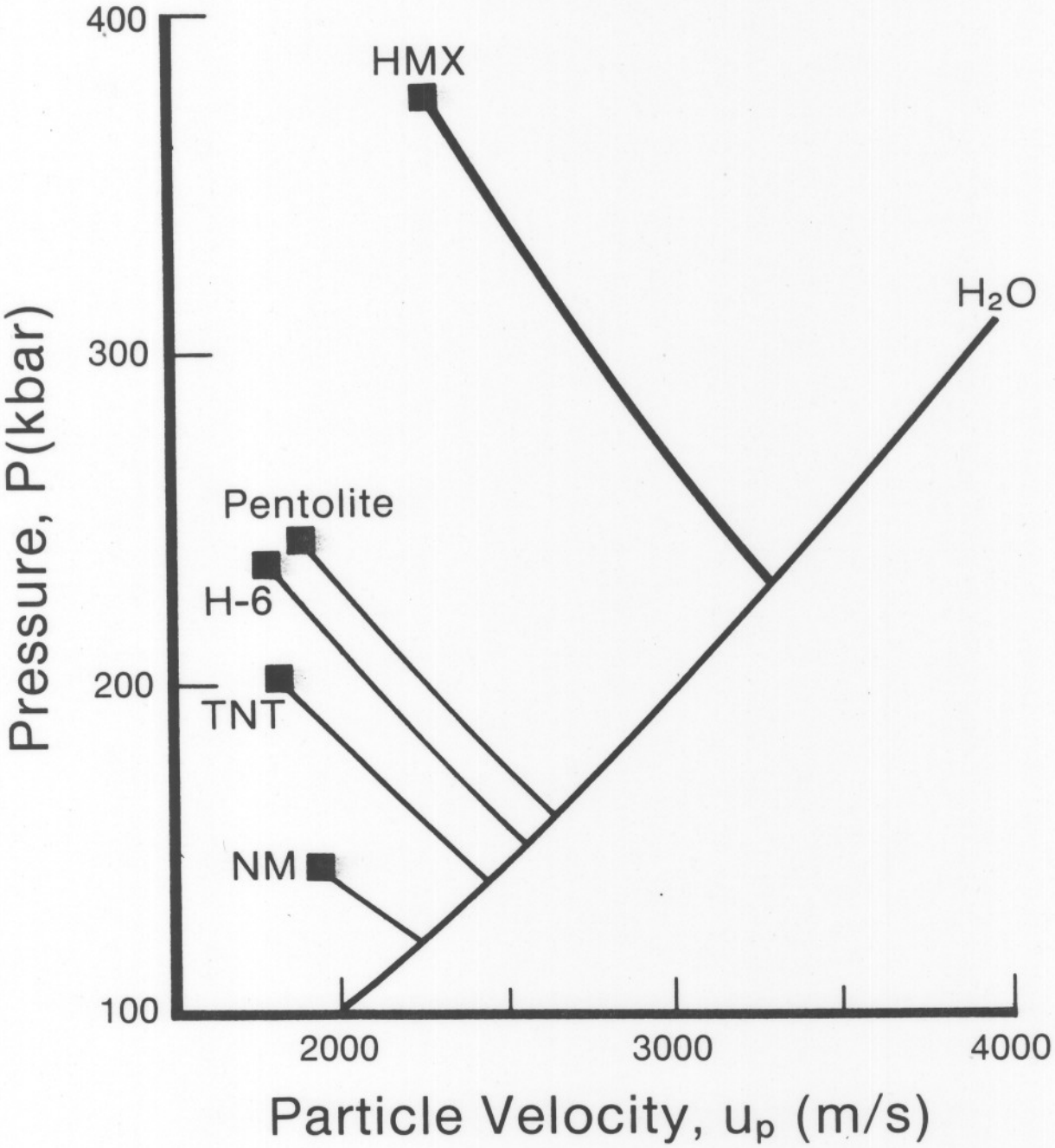

Figure 6. Pressure–velocity solutions for the detonation of 5 conventional explosives at maximum initial densities.

Table 1. CJ conditions and interface pressure for five explosives detonating in water.

HE	ρ_o (g/cm^3)	Δh_{det} (MJ/kg)	P_{CJ} (kbar)	P_I (kbar)	ΔS (kJ/kg-K)	P_σ (bar)
HMX	1.89	6.19	388	230	3.6	140
Pentolite	1.67	5.86	249	160	2.8	40
H-6	1.75	–	221	151	2.7	35
TNT	1.65	5.40	202	140	2.5	22
NM	1.13	5.69	144	121	2.0	8

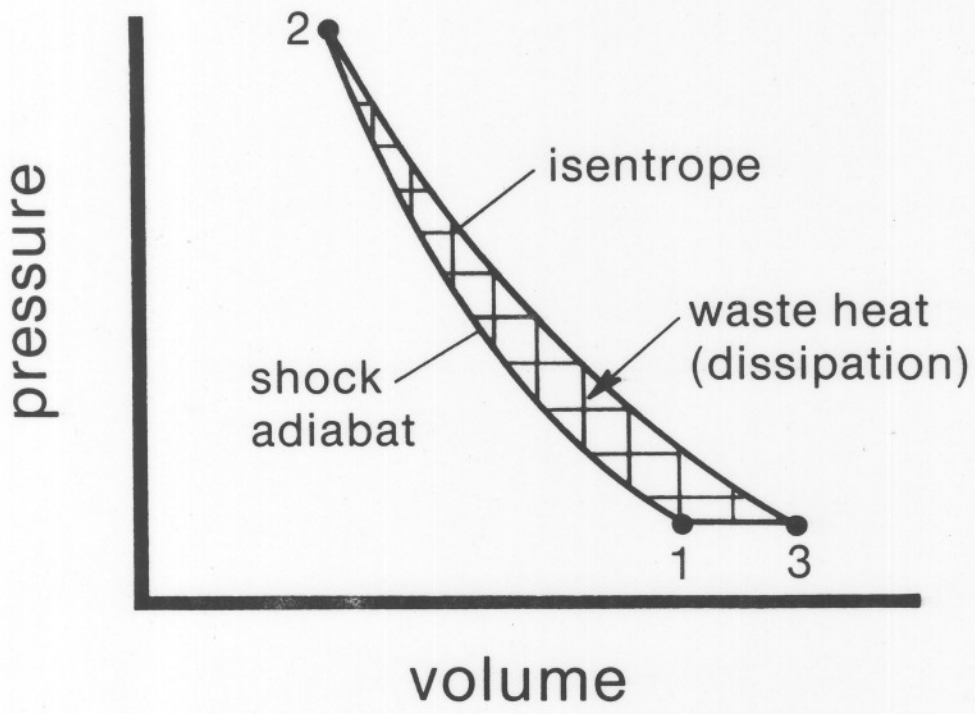

Figure 7. Shock adiabat (hugoniot) vs isentrope in pressure–volume coordinates. Shaded area is the waste heat (dissipated energy) that is not recovered when the shock pressure is released back to ambient.

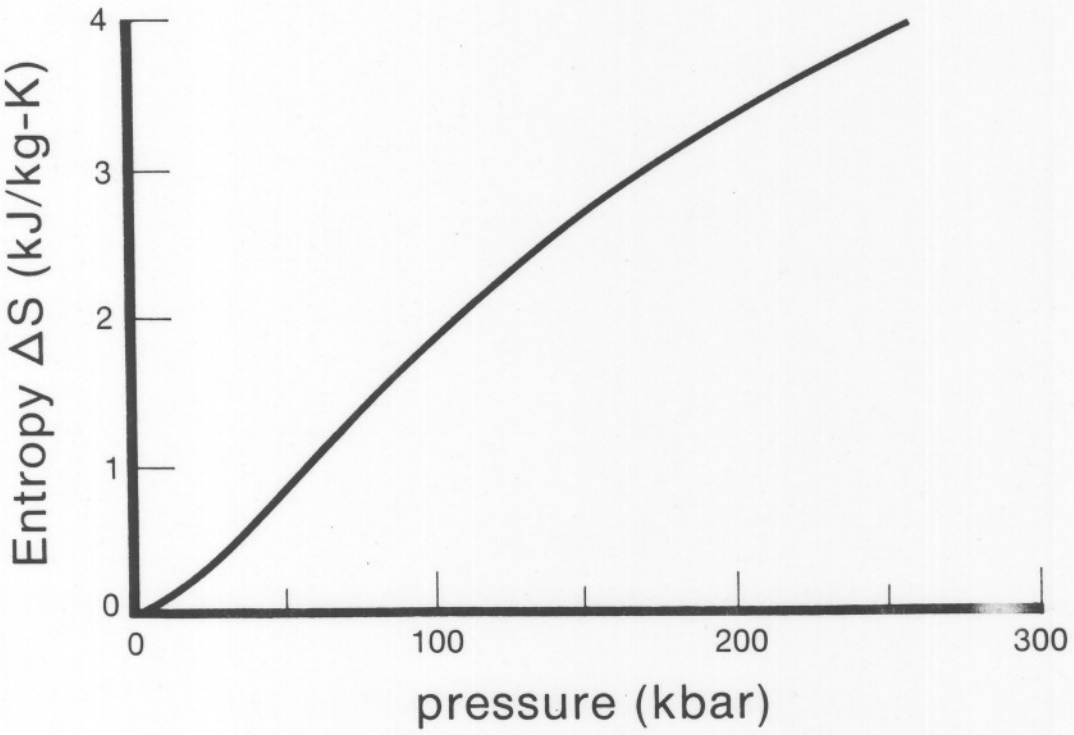

Figure 8. Entropy jump across shock wave vs shock pressure for water, initial conditions of 300 K and 1 bar.

(a). Pentolite, centrally detonated

(b). PBX 9404, centrally detonated

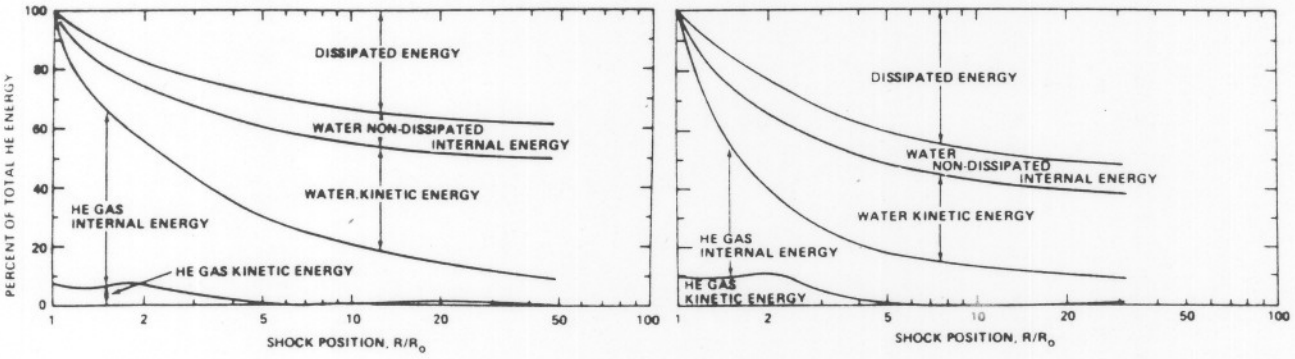

(c). Pentolite constant volume explosion, $\rho_O = 1.65$.

(d). Pentolite constant volume explosion, $\rho_O = 0.4125$.

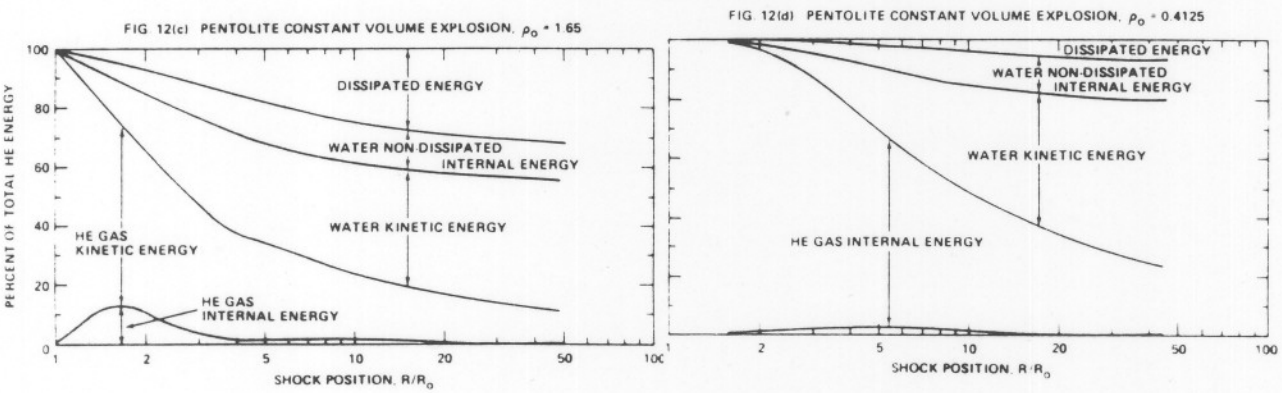

Figure 9. Energy budgets for four explosives. From Hurwitz and Sternberg.[11]

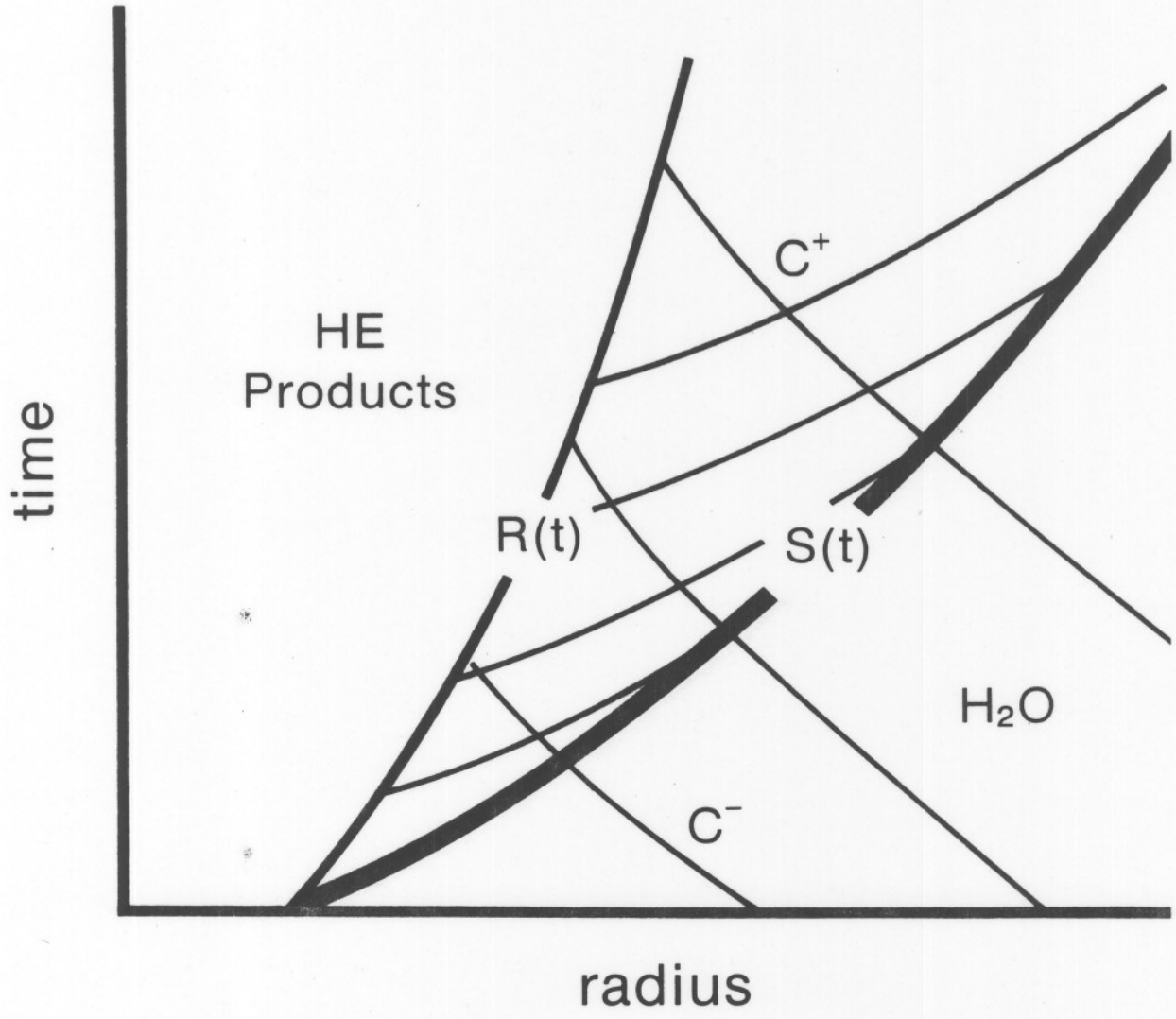

Figure 10. Interaction of acoustic waves with shock. Information about the interface motion is transmitted forward along the characteristics C^+ and the reflected waves are transmitted back along C^-.

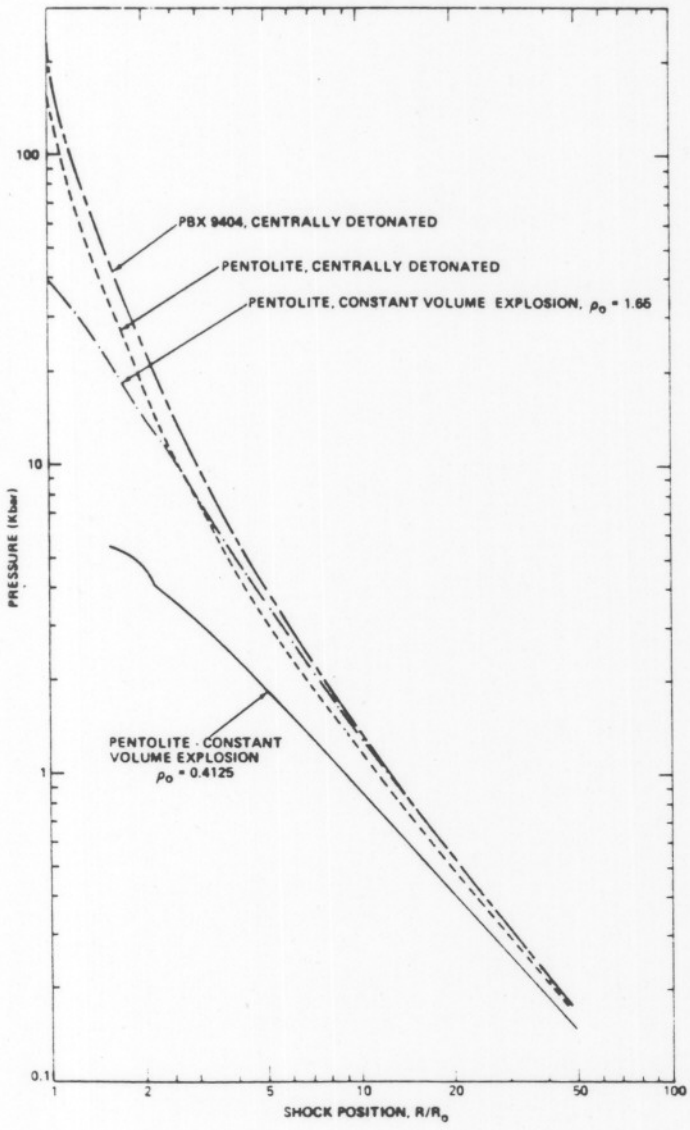

Figure 11. Decay of shock pressure with scaled distance for the four cases shown in Fig. 9. From Sternberg and Hurwitz.[12]

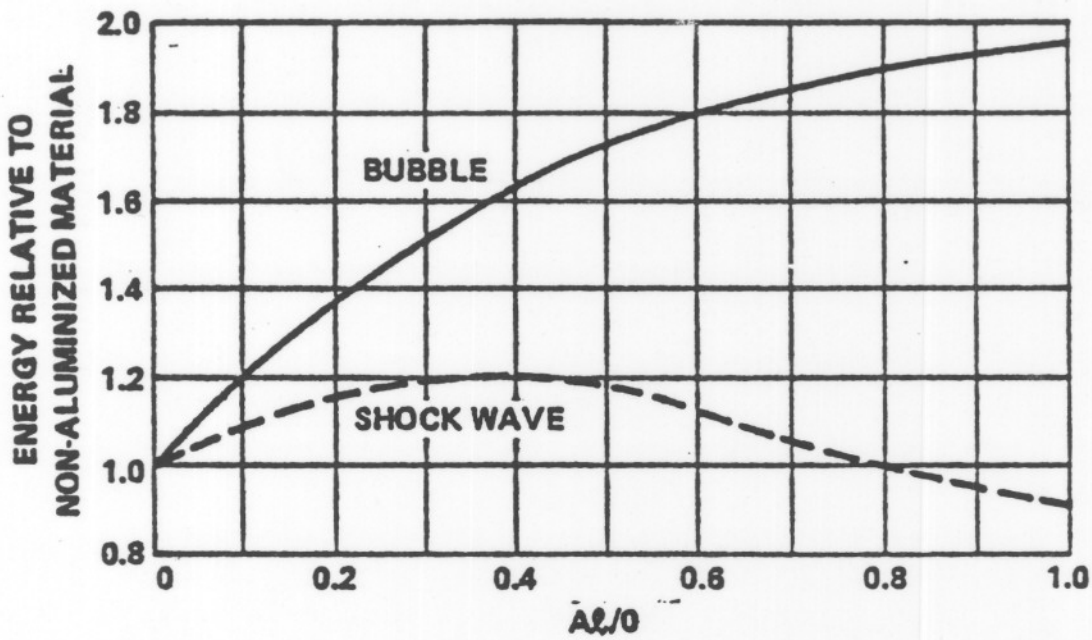

Figure 12. Effect of the addition of aluminum to conventional CHNO explosives. From Swisdak, Ref. 3. A molar Al/O ratio of 0.242 corresponds to a 15 wt % (0.59 mol %) Al in a RDX/Al mixture; a molar Al/O ratio of 0.587 corresponds to a 30 wt % (0.78 mol %) Al in a RDX/Al mixture.)

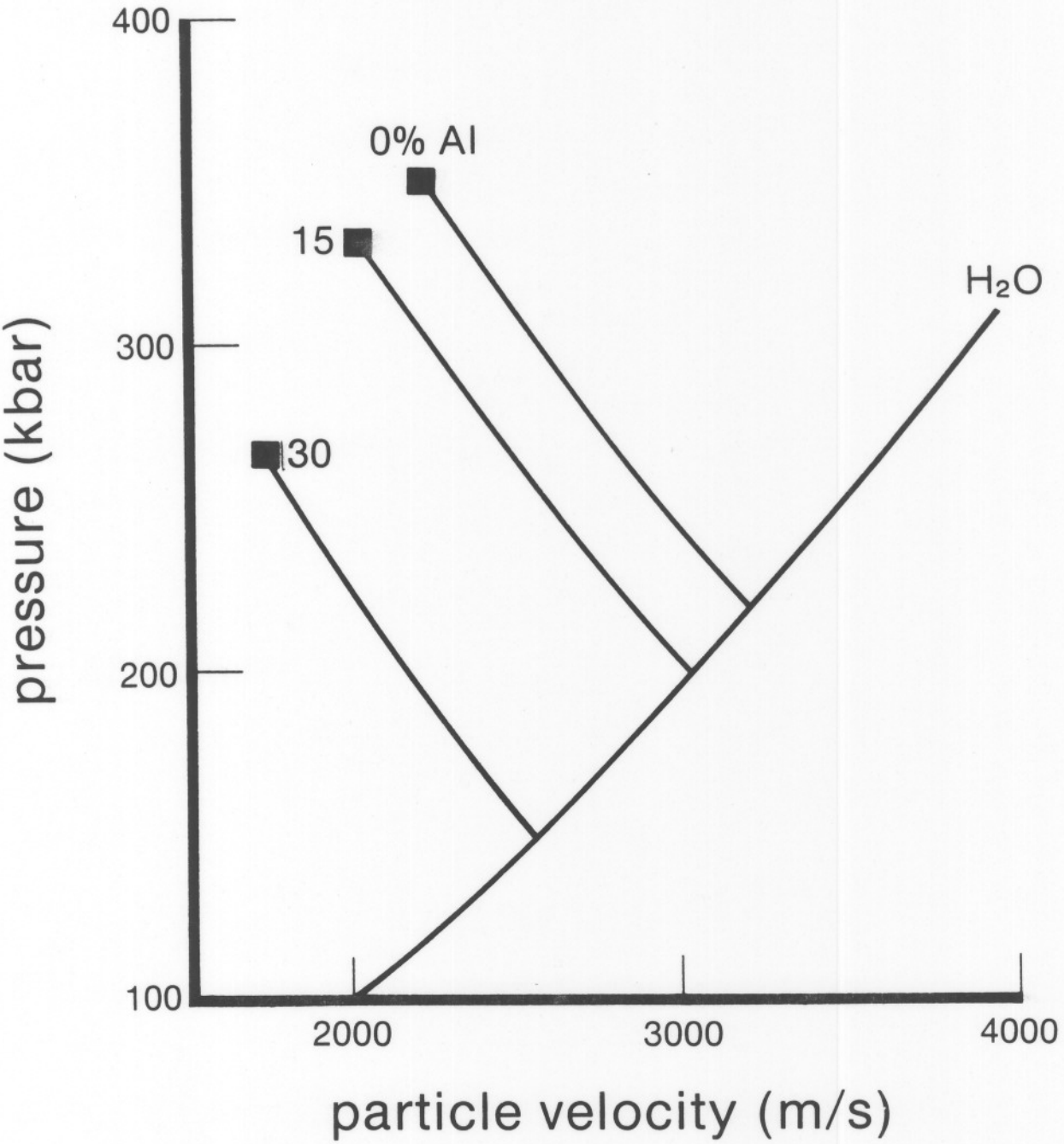

Figure 13. Detonation–water interface interaction solutions for RDX/Al explosive mixtures. Products include condensed aluminum oxide Al_2O_3(s) and graphitic carbon C(s). RDX alone has CJ parameters similar to but slightly lower than HMX.

Table 2. CJ conditions and interface pressure for RDX/Al explosive mixtures detonating in water.

Al (wt %)	ρ_o (g/cm^3)	Δh_{det} (MJ/kg)	P_{CJ} (kbar)	P_I (kbar)	ΔS (kJ/kg-K)	P_σ (bar)
0	1.80	6.15	349	220	3.5	123
15	1.90	8.21	331	200	3.4	102
30	2.00	10.12	267	150	2.7	35

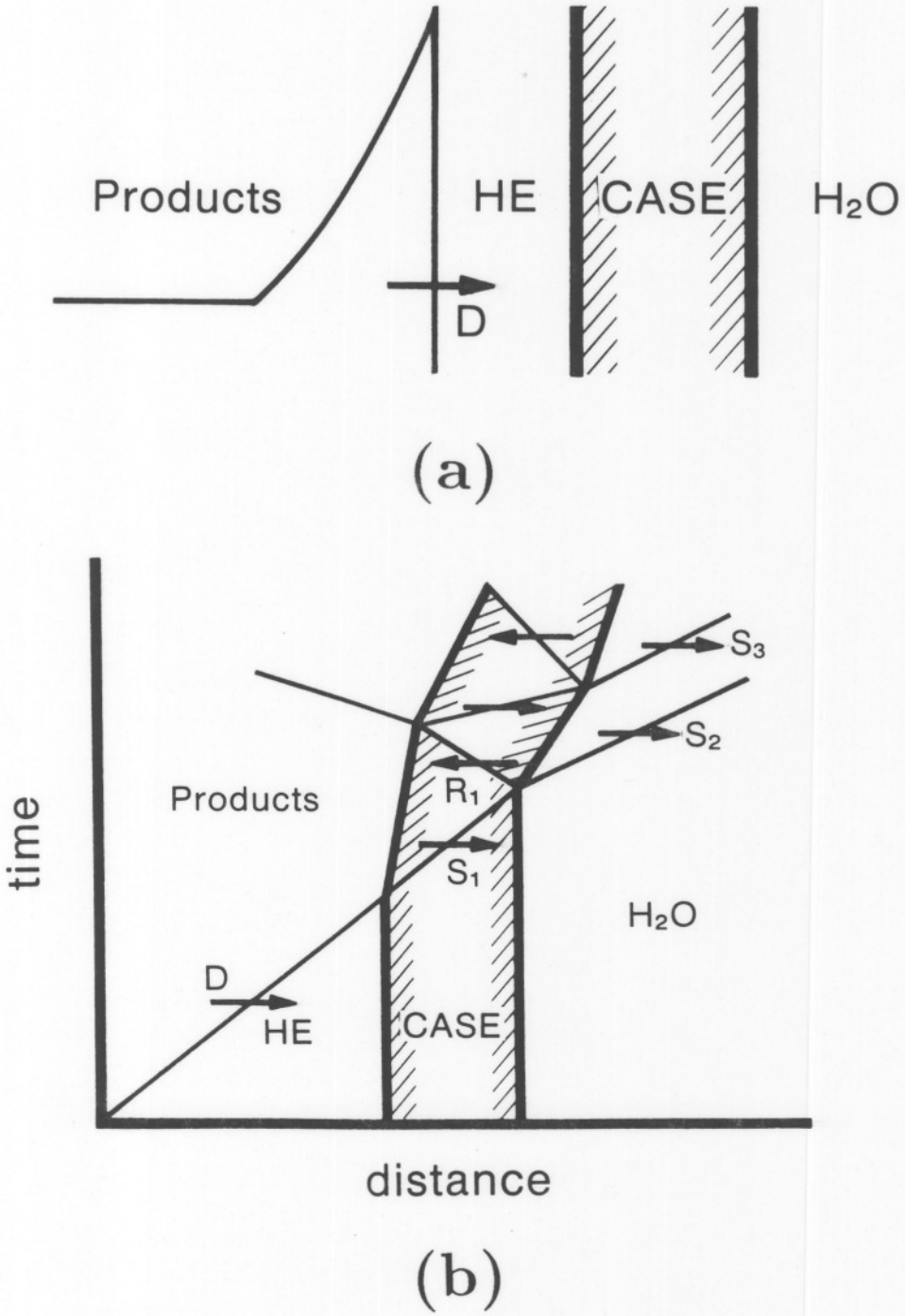

Figure 14. Detonation–case–water interaction. (a) spatial configuration. (b) distance–time diagram showing multiple reflections.

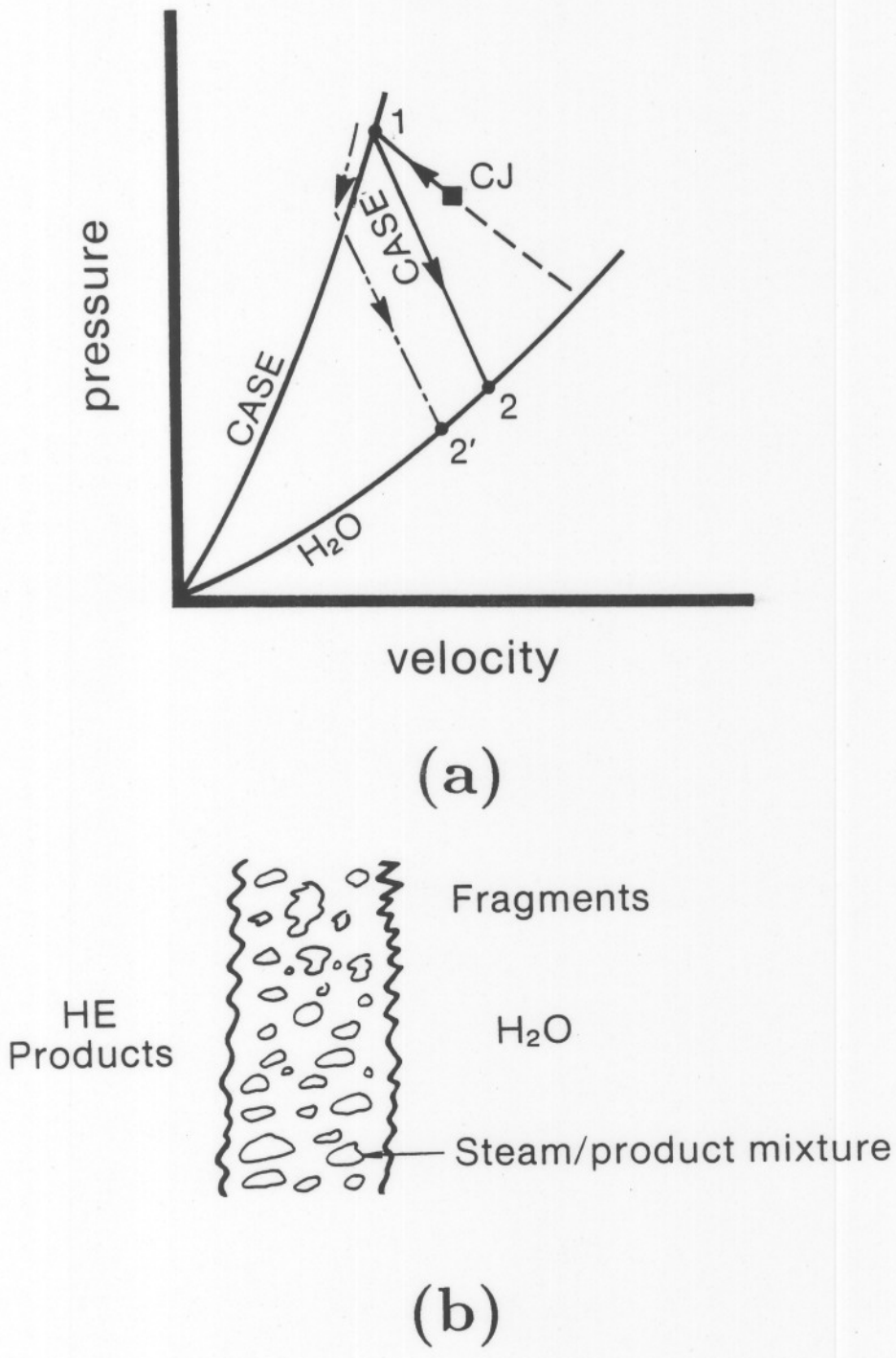

Figure 15. Detonation–case–water interaction. (a) pressure-velocity solution for interface conditions. (b) extended interface generated by case fragmentation; interface region is a mixture of fragments, steam and liquid water.

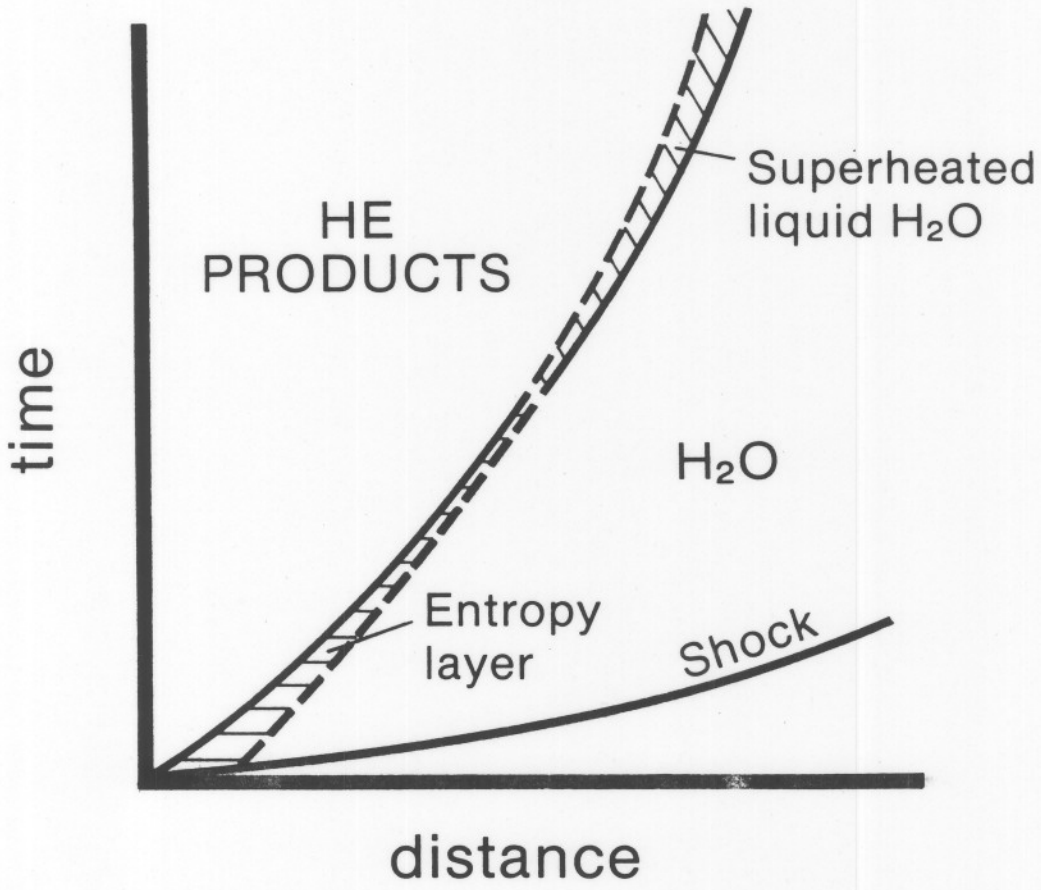

Figure 16. Distance–time diagram showing the formation of the entropy layer and the transformation into superheated water with decreasing interface pressure or increasing time.

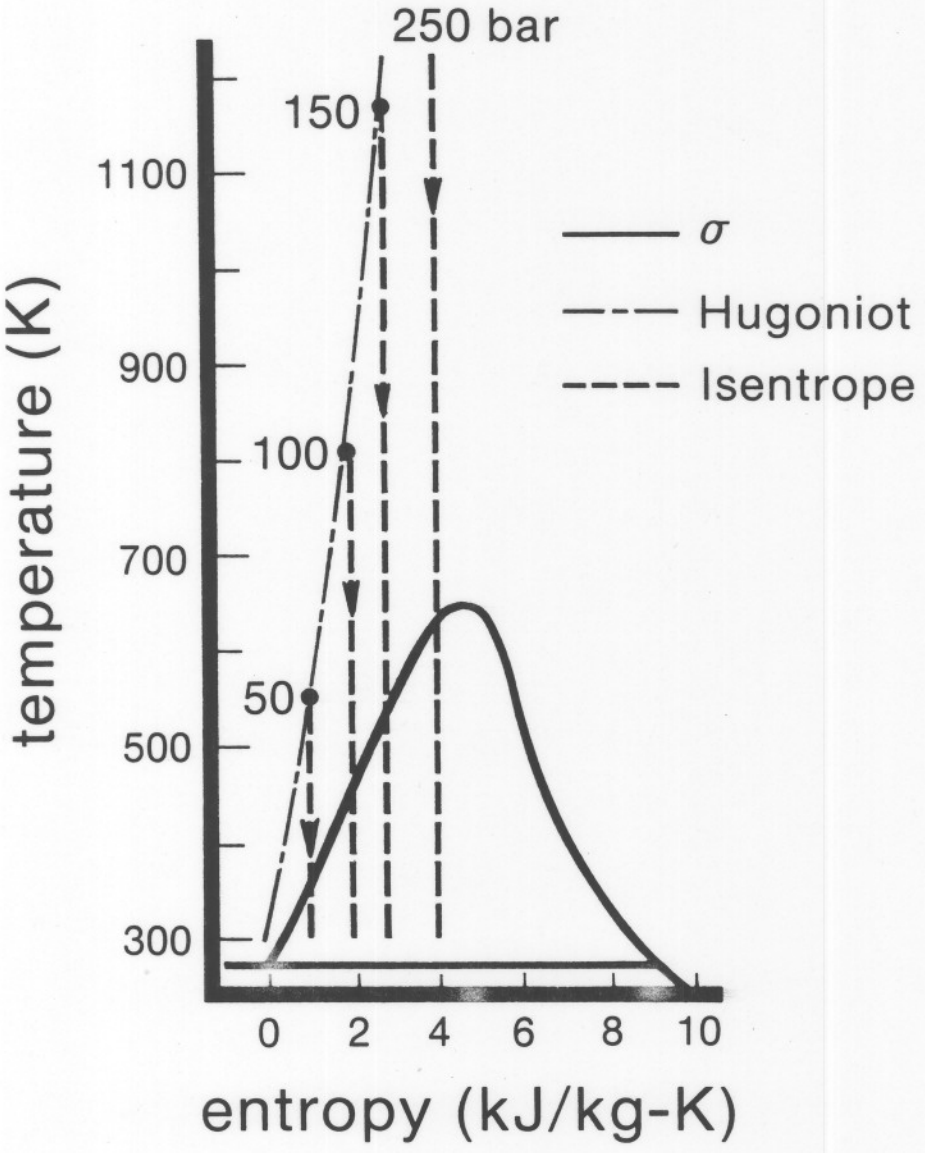

Figure 17. Temperature–entropy diagram for water. The chain-dotted line is the shock adiabat (hugoniot) with the shock pressure indicated at 50, 100, and 150 kbar (250 kbar is off scale), initial water conditions of 300 K and 1 atm. The dashed lines are the isentropes, and the heavy line is the liquid–vapor coexistence curve σ.

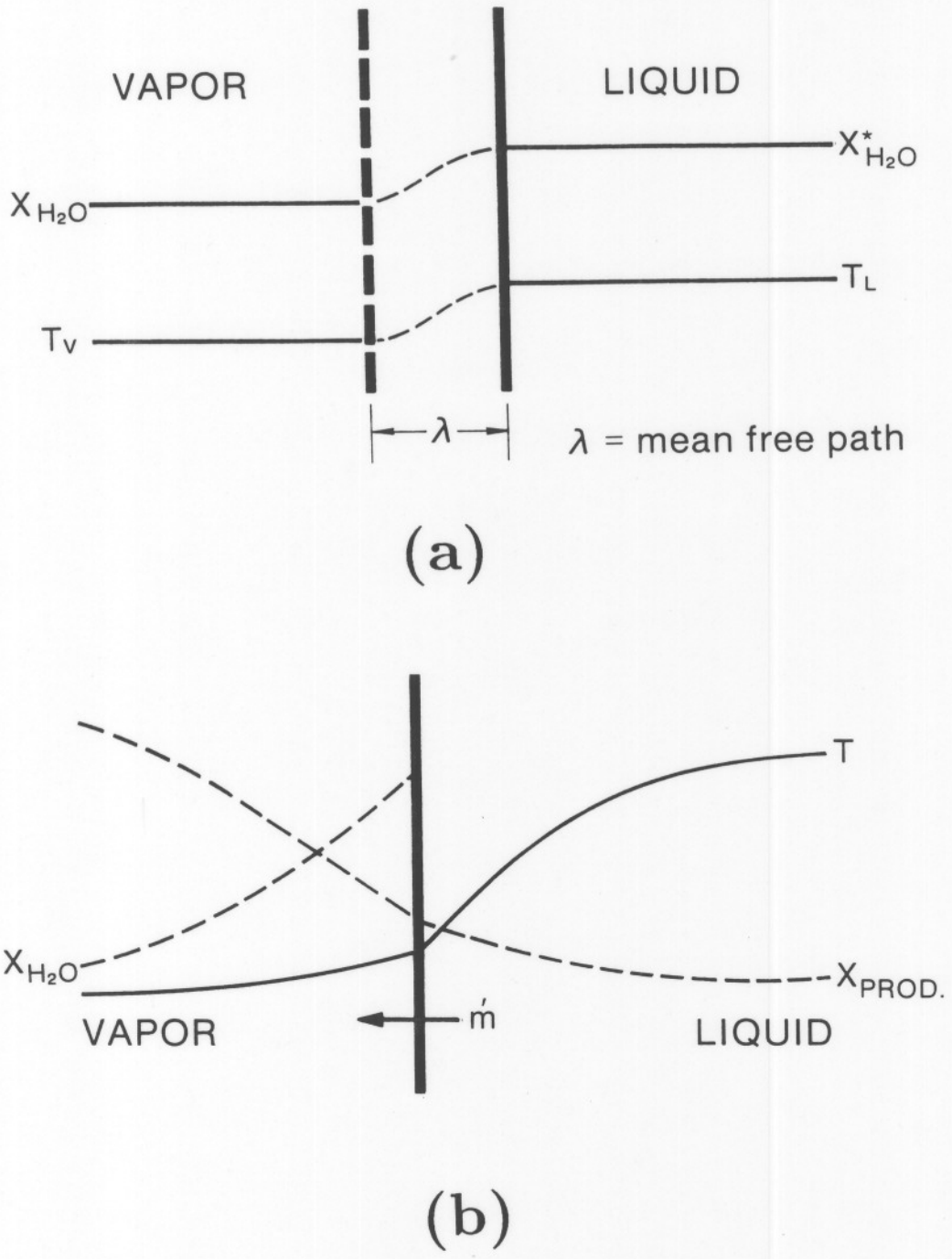

Figure 18. Evaporating interface configuration. (a) near–equilibrium situation: mass and energy boundary layers control evaporation rates. (b) nonequilibrium situation: rapid evaporation with large state variations occurring in the Knudsen layer at the interface.

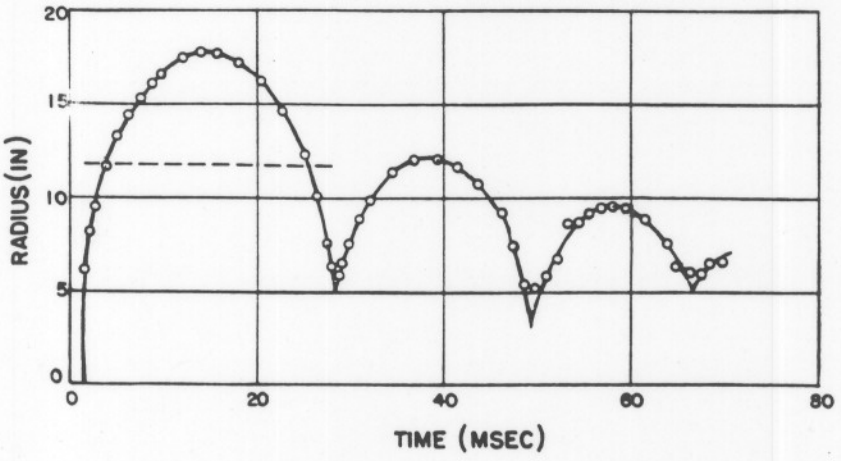

(a)

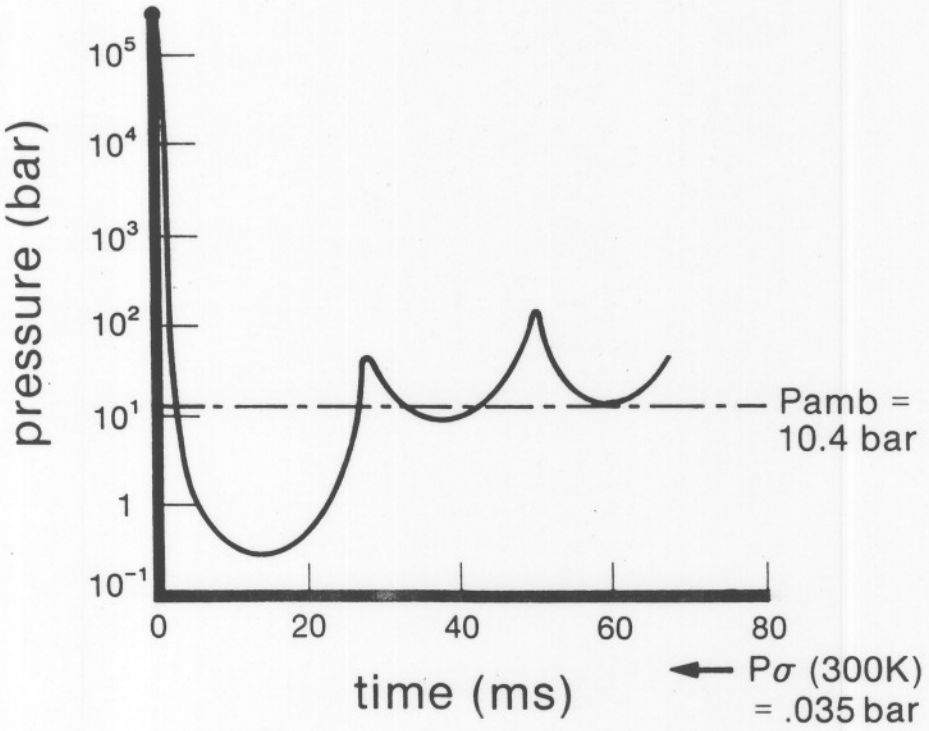

(b)

Figure 19. Explosion bubble produced by the detonation of 250 g (R_o = 1.38 in) of tetryl at a depth of 300 ft. (a) Observed radial oscillations. (b) Computed (using JWL isentrope) average pressure oscillation inside the bubble (and at the interface).

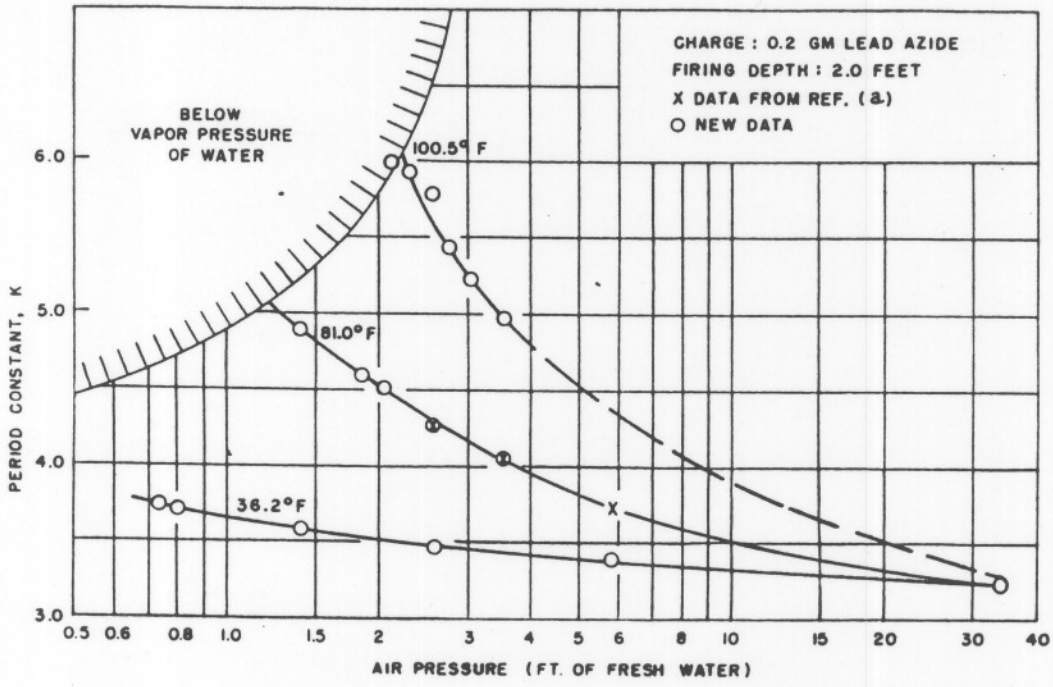

Figure 20. Effect of ambient water temperature on the bubble period constant K (English units). From Ref. 26

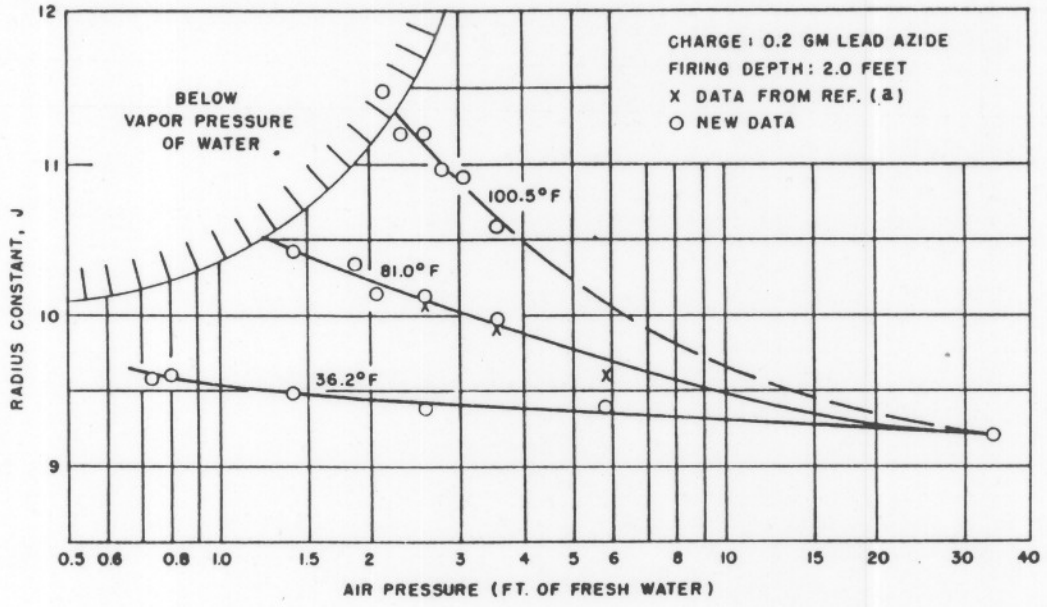

Figure 21. Effect of ambient water temperature on the bubble maximum radius constant J (English units). From Ref. 26

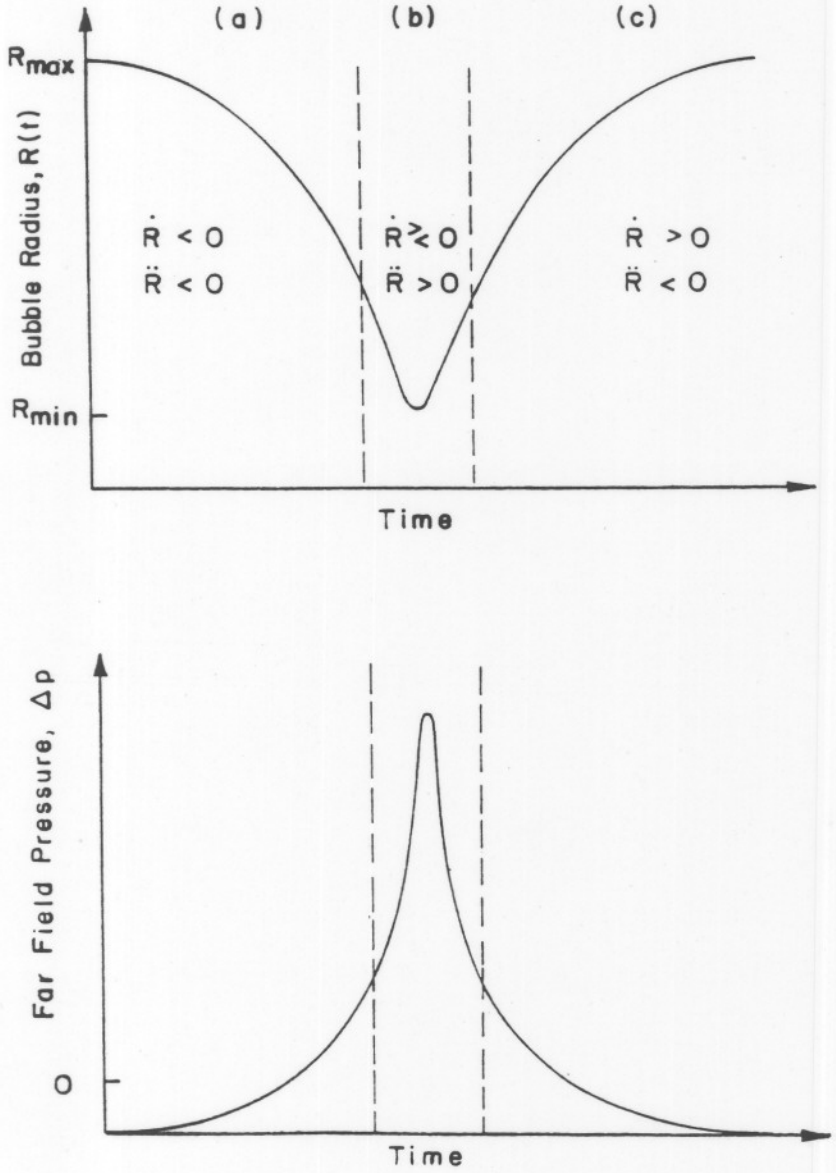

Figure 22. Bubble surface motion and resulting pressure wave. The region of potential Rayleigh–Taylor instability is near the minimum radius where the accelerations are large and positive.